



**HAL**  
open science

## The SAFRAN-ISBA-MODCOU hydrometeorological model applied over France

Florence Habets, Aaron Boone, Jean-Louis Champeaux, Pierre Etchevers, Laurent Franchisteguy, Etienne Leblois, Emmanuel Ledoux, Patrick Le Moigne, Eric Martin, Sophie Morel, et al.

### ► To cite this version:

Florence Habets, Aaron Boone, Jean-Louis Champeaux, Pierre Etchevers, Laurent Franchisteguy, et al.. The SAFRAN-ISBA-MODCOU hydrometeorological model applied over France. *Journal of Geophysical Research: Atmospheres*, 2008, 113 (D06113), pp.18. 10.1029/2007JD008548 . meteo-00274446

**HAL Id: meteo-00274446**

**<https://meteofrance.hal.science/meteo-00274446v1>**

Submitted on 18 Apr 2008

**HAL** is a multi-disciplinary open access archive for the deposit and dissemination of scientific research documents, whether they are published or not. The documents may come from teaching and research institutions in France or abroad, or from public or private research centers.

L'archive ouverte pluridisciplinaire **HAL**, est destinée au dépôt et à la diffusion de documents scientifiques de niveau recherche, publiés ou non, émanant des établissements d'enseignement et de recherche français ou étrangers, des laboratoires publics ou privés.

# **1 The SAFRAN-ISBA-MODCOU hydrometeorological 2 model applied over France**

F. Habets,<sup>1</sup> A. Boone,<sup>2</sup> J.L Champeaux<sup>2</sup>, P. Etchevers<sup>3</sup>, L. Franchistéguy,<sup>2</sup> E.

Leblois,<sup>4</sup> E. Ledoux,<sup>5</sup> P. Le Moigne,<sup>2</sup> E. Martin<sup>2</sup>, S. Morel,<sup>6</sup> J. Noilhan,<sup>2</sup> P.

Quintana Seguí,<sup>2</sup> F. Rousset-Regimbeau,<sup>2</sup> P. Viennot<sup>5</sup>

<sup>3</sup> 1GAME/CNRM (Météo-France, CNRS) Toulouse, France, now at UMR-Sisyphe 7619 (Uni-  
<sup>4</sup> versit Paris VI, CNRS) Paris, France 2GAME/CNRM (Météo-France, CNRS) Toulouse, France  
<sup>5</sup> 3GAME/CEN (Météo-France, CNRS), Saint Martin d’Heres, France 4CEMAGREF, Lyon, France  
<sup>6</sup> 5Centre de Geosciences (ENSMP, ParisTech), Fontainebleau, France 6DIRIC, Météo-France,  
<sup>7</sup> Paris, France

---

Florence Habets, UMR-Sisyphe 7619 - ENSMP, 35 rue St Honoré, 77305 Fontainebleau, France.

(florence.habets@ensmp.fr)

8 Abstract. The hydrometeorological model SIM consists in a meteorological  
9 analysis system (SAFRAN), a land surface model (ISBA) and a hydrogeo-  
10 logical model (MODCOU). It generates atmospheric forcing at an hourly time  
11 step, and it computes water and surface energy budgets, the riverflow at more  
12 than 900 rivergauging stations, and the level of several aquifers. SIM was ex-  
13 tended over all of France in order to have a homogeneous nation-wide mon-  
14 itoring of the water resources: it can therefore be used to forecast flood risk  
15 and to monitor drought risk over the entire nation.

16 The hydrometeorological model was applied over a 10-year period from 1995  
17 to 2005. In this paper the databases used by the SIM model are presented,  
18 then the 10-year simulation is assessed by using the observations of daily stream-  
19 flow, piezometric head, and snow depth. This assessment shows that SIM is  
20 able to reproduce the spatial and temporal variabilities of the water fluxes.  
21 The efficiency is above 0.55 (reasonable results) for 66 % of the simulated  
22 rivergages, and above 0.65 (rather good results) for 36 % of them. However,  
23 the SIM system produces worse results during the driest years, which is more  
24 likely due to the fact that only few aquifers are simulated explicitly. The an-  
25 nual evolution of the snow depth is well reproduced, with a square correla-  
26 tion coefficient around 0.9 over the large altitude range in the domain. The  
27 streamflow observations were used to estimate the overall error of the sim-  
28 ulated latent heat flux, which was estimated to be less than 4 %.

## 1. Introduction

29 Interfacing a Soil Vegetation Atmosphere Transfert Scheme (SVAT) with streamflow  
30 routing model permits the assessment of the water and energy budgets simulated by  
31 SVAT schemes, and the identification of their main qualities and defects. This has been  
32 done extensively in order to assess global and regional climate models (Miller et al., 1994,  
33 Benoit et al., 2000), as well as in SVAT intercomparison experiments. For instance, the  
34 Pilps2c experiment (Wood et al., 1998, Lohmann et al., 1998) showed the importance of  
35 the parameterization of subgrid runoff for simulating a realistic hydrograph. The Rhone-  
36 Agg intercomparison study (Boone et al., 2004) showed that in the Alps, the SVATs  
37 that use explicit snow schemes (with an explicit simulation of the energy budget of the  
38 snowpack) obtain better results than those using composite snow schemes (i.e. one single  
39 energy budget for both the snow-free and snow covered part of the ground surface).  
40 Results of the DMIP1 (distributed model intercomparison model, Reed et al., 2004) show  
41 that among the participant distributed hydrological models, the few that simulated both  
42 the water and the energy budgets (NOAH, Chen et al., 1997; VIC-3L, Liang et al., 1994;  
43 and tRIBS, Ivanov et al., 2004) obtained similar results in terms of the simulation of  
44 the riverflows as the others. Thus, although SVAT schemes were originally dedicated to  
45 providing surface energy fluxes to an atmosphere model, they are now also able to make  
46 an accurate estimation of the hydrological cycle at both short and long time scales.

47 Several studies focusing on the soil moisture assimilation for numerical weather predic-  
48 tion models have used SVAT off-line simulations (i.e. uncoupled to the atmosphere) forced  
49 by observed data, in combination with satellite and/or surface atmospheric data assimi-

50 lation to estimate mesoscale soil moisture over large areas (ELDAS, European Land Data  
51 Assimilation System, Van den Hurk et al., 2005, NLDAS, North-American Land Data  
52 Assimilation System, Mitchell et al., 2004). One key aspect of such studies is the retrieval  
53 of the best surface near-realtime atmospheric forcing. However, both studies include a  
54 retrospective period in order to test the ability of the method to compute consistent sur-  
55 face fluxes and riverflow over long time periods. In NLDAS, the SVAT schemes are also  
56 coupled to a hydrological routing model in order to assess the SVAT scheme simulations  
57 of the water budget over large areas, through comparison with observed riverflows.

58 The CNRM-GAME has been developing SVAT scheme and soil moisture assimilation  
59 techniques for over the last ten years, in order to provide surface boundary conditions  
60 to the atmosphere models. For instance, CNRM-GAME takes part in the ELDAS and  
61 CALDAS (Balsamo et al., 2006) projects using the ISBA surface scheme. It has also,  
62 in association with the Mining school of Paris, developed the SIM hydrometeorological  
63 model that is used both for realtime estimation of the soil moisture, and for retrospective  
64 studies of the water and energy budgets for a region covering all of France.

65 The SIM (SAFRAN-ISBA-MODCOU) model is the combination of three independant  
66 parts: i) SAFRAN (Durand et al., 1992), which provides an analysis of the atmospheric  
67 forcing, ii) ISBA (Noilhan et Planton 1989, Boone et al., 1999), which computes the surface  
68 water and energy budgets, and iii) MODCOU (Ledoux et al., 1989), which computes the  
69 evolution of the aquifers and the riverflow.

70 The SIM system was first tested for large French catchments: the Adour (Habets et  
71 al., 1999c), the Rhone (Etchevers et al., 2001), the Garonne (Voirin-Morel, 2003) and the  
72 Seine basins (Rousset et al., 2004), and the Maritsa river basin in Bulgaria (Artinyan et

73 al., 2007). It has been used to quantify the influence of the snowpack, groundwater, soil  
74 moisture, and urbanised areas on certain flood events of the Seine basin (Rousset et al.,  
75 2004). SIM has also been used to study the evolution of the water resources in a climate  
76 change prospective (Etchevers et al., 2002, Caballero et al., 2007).

77 SIM was extended over all of France in 2002, and it has been used operationally at  
78 Meteo-France since 2003 in order to monitor the water resources at the national scale in  
79 near real-time. In order to assess the quality of the SIM system over France, a retrospective  
80 run was made for the period 1995 to 2005, and the goal of this article is to present the  
81 results of the SIM hydrometeorological model over this period. First, the SIM system  
82 is presented, with a summary of the main innovations compared to the previous studies.  
83 Then, the database is presented, with a special emphasis on the atmospheric data, which  
84 is critical in terms of the quality of the entire system. The assessment is based on observed  
85 riverflow, piezometric head, and snow depth. Finally, the spatial and temporal evolutions  
86 of the water and energy fluxes on the main basins are presented.

## 2. The SIM hydrometeorological model

87 The SIM (SAFRAN-ISBA-MODCOU) system consists in 3 independent modules (figure  
88 1):

- 89 • The SAFRAN analysis system (Durand et al., 1992) was developed in order to provide  
90 an analysis of the atmospheric forcing in mountainous areas for the avalanche forecasting.  
91 SAFRAN analyses 8 parameters: the 10m wind speed, 2m relative humidity, 2m air  
92 temperature, cloudiness, incoming solar and atmospheric radiations, snowfall and rainfall.  
93 A detailed description and assessment of the SAFRAN analysis over France is presented  
94 in Quintana-Seguí et al., 2007, so that only the main aspects are summarized herein.

95 The main hypothesis of SAFRAN is that the atmospheric variables are considered to be  
96 homogeneous over some well-defined areas, within which they can only vary according  
97 to the topography. In France, these areas correspond to the Symposium homogeneous  
98 climate zones which are used at Meteo-France for weather forecast bulletins. There are  
99 about 600 homogeneous climate zones, each with an average area around of  $1000 \text{ km}^2$ , so  
100 that each zone contains at least two raingages and one surface meteorologic station.

101 SAFRAN takes into account all of the observed data in and around the area under study.  
102 For instance, there are more than 1000 meteorological stations for the 2m temperature and  
103 humidity, and more than 3500 daily raingages, which corresponds to about 6 raingages  
104 for each climate zone. For each variable analysed, an optimal interpolation method is  
105 used to assign values to given altitudes within the zone. According to the altitude of the  
106 observations, SAFRAN provides a single vertical profile of the variable within the zone  
107 with a vertical resolution of 300m.

108 The analysis are computed every 6 hours, and the data are interpolated to a hourly time  
109 step.

110 The incoming radiative fluxes, and the precipitation (liquid and solid) are treated differ-  
111 ently.

112 The precipitation rate is estimated daily using 3500 daily raingages, and then interpolated  
113 hourly, based on the evolution of the air relative humidity (precipitation is constrained  
114 to occur when the relative humidity is high). The partition between snowfall and rainfall  
115 is based on the  $0.5^\circ\text{C}$  isotherm: the precipitation is considered as snowfall if the air  
116 temperature is below  $0.5^\circ\text{C}$ .

117 The radiation scheme of Ritter and Geyley (1992) is used to compute the incoming ra-  
118 diation fluxes since there are few in-situ observations available. The method requires an  
119 estimate of the cloudiness which is analysed using, as a first guess, the operational analysis  
120 of Numerical Weather Prediction model, and in-situ observations.

121 Once the vertical profile of the atmospheric parameters have been computed in each  
122 homogeneous zone, the values are interpolated in space as a function of the altitude of  
123 each gridcell within each homogeneous zone.

124 • The ISBA land surface scheme (Noilhan et Planton, 1989, Noilhan and Mahfouf,  
125 1996) is used in the NWP, research and climate models at Meteo-France. In order to  
126 fulfill all its applications, the ISBA surface scheme is quite modular. In the SIM system,  
127 the 3-layer force restore model is used (Boone et al., 1999), together with the explicit  
128 multi-layer snow model (Boone et al., 2001). Moreover, the subgrid runoff (Habets et  
129 al., 1999b) and subgrid drainage schemes (Habets et al., 1999a) are used. This last  
130 parametrisation is quite simple, and allow to indirectly take into account the impact of  
131 unresolved aquifers on the low riferflows based on a single parameter.

132 The soil and vegetation parameters used by ISBA are derived from the ECOCLIMAP  
133 database (Masson et al., 2003, see section 3.2). Only two parameters in ISBA are not  
134 directly defined by the soil and vegetation classification: the subgrid runoff parameter  
135 and the subgrid drainage parameter,  $w_{drain}$ .

The subgrid runoff parameter was assigned the default value in the current study as  
was the case for the other SIM applications. Only the subgrid drainage parameter was  
calibrated in this application. In previous simulations, this subgrid parameter was either  
set to a default value (Habets et al., 1999a), or calibrated to optimize the Nash criteria



(Etchevers et al., 2001), or the discharge for the summer low flow period (Caballero et al., 2007). In the France application, it is calibrated using the method presented in Caballero et al., (2007) in order to sustain the observed Q10 quantile of the riverflow. The subgrid drainage parameter is simply set using the expression

$$Q10 = \sum_i C_{3i}/\tau \times w_{drain} \times d_i \times S_i$$

136 where  $i$  represents the gridcells that belong to the upstream area of the rivergagge under  
137 study,  $C_{3i}$  is the gravitational drainage coefficient for the gridcell  $i$ ,  $d_i$  the soil depth for  
138 the gridcell  $i$ ,  $S_i$  is the surface of the gridcell  $i$  that belong to the upstream area of the  
139 rivergagge under study, and  $\tau$  a time constant of one day. In this expression,  $C_{3i}$  and  
140  $d_i$  only depend on the soil and vegetation database, and  $Q10$  is set at each simulated  
141 rivergagge using the statistics provided over the entire observation period for each station.  
142 Thus, the value of the subgrid drainage coefficient is defined using observed data and the  
143 physiographic database, and is thus unique once these databases are defined. Therefore,  
144 there is no iteration for the calibration, and thus, no "calibration period"

145 The surface scheme is linked to the MODCOU hydrogeological model by the ISBA output  
146 soil water fluxes: The drainage simulated by ISBA is transfered to MODCOU as the input  
147 flow for the simulation of the evolution of the aquifer, while the surface runoff computed by  
148 ISBA is routed within the hydrographical network by MODCOU to compute the riverflow.

149 • The MODCOU hydrogeological model computes the spatial and temporal evolution  
150 of the piezometric level of multilayer aquifers, using the diffusivity equation (Ledoux et al.,  
151 1989). It then computes the exchanges between the aquifers and rivers, and finally it routes  
152 the surface water within the river, using a simple isochronism algorithm (Muskingum), to  
153 compute riveflows. In the SIM-France system, the riverflow is computed at a 3-hour time

154 step (instead of daily as in the previous applications), and the evolution of the aquifer is  
155 computed daily.

156 ISBA snowpack, soil temperature and soil moisture values are initialised using a one year  
157 spin-up (the first year is repeated twice), whereas, the initial conditions of the aquifers  
158 are taken from the Rhone and Seine basin applications.

159 In the next section, a short description of the database is presented.

### 3. Databases used

160 The databases for the SIM-France application use the Lambert II projection, which has  
161 the advantage of preserving the surface area. SIM uses input data that have different  
162 spatial resolutions: a regular 8 km grid is used by SAFRAN and ISBA, and irregular  
163 embedded gridcells varying in size from 1 to 8 km are used by MODCOU (the highest  
164 resolution is associated with rivers and basin boundaries).

#### 3.1. Hydrogeologic database

165 The hydrographic network was derived from the USGS GTOPO30 elevation database  
166 at a 1 km resolution. The slope is used to derive the direction of the flow, and to compute  
167 the drainage area of each cell.

168 The topography at the 8 km resolution, the river network, and the main basins are shown  
169 in figure 2. The river network extends over approximately 42000 km, which represents  
170 about 12% of the 194000 mesh points of the hydrographic network.

171 More than 900 rivergages are taken into account in the riverlfow simulations, with an  
172 upstream area ranging from 240  $km^2$  to 112000 $km^2$ .

173 Currently the aquifers of only two basins have been simulated: the 3 aquifer layers of  
174 the Seine basin, and the single aquifer layer of the Rhone basin (figure 3). The aquifer  
175 parameters were calibrated by Gomez et al., (2003), and Golaz et al., (2001), respectively,  
176 and were already used in previous applications of SIM for these basins.

177 However, aquifers are more widespread in France. The main aquifers defined in the  
178 French Hydrogeological Reference database (BD RHF, <http://sandre.eaufrance.fr> ) and  
179 those simulated are shown in figure 3. In those areas where an aquifer is present but not  
180 explicitly simulated (grey shaded areas in figure 3), the subgrid drainage parameter was  
181 calibrated in order to sustain the summer riverflows. Everywhere else, the parameter is  
182 set to 0.

### 3.2. Soil and Vegetation parameters for ISBA

183 The ISBA parameters are derived from the ECOCLIMAP database (Masson et al.,  
184 2003). However, an improved version of the ECOCLIMAP database was developed for  
185 the SIM application.

186 This database uses a Lambert II projection at a 1 km resolution for both the vegetation  
187 and the soil parameters (as opposed to approximately 10km for the soil map in the global  
188 ECOCLIMAP database).

189 The vegetation classification (figure 4) is based on the Corine Land Cover CLC 1990  
190 database, associated with a climate map (Masson et al., 2003). This database is quite  
191 accurate for the forested areas, vineyards and urban areas, but it does not distinguish  
192 the various crops that are aggregated into a single class and distributed over very large  
193 domains. In order to be able to distinguish winter and summer crops, as was done in the  
194 Adour study (Habets et al., 1999b), it was decided to better define the crop classes, using

195 the 10-day NDVI (Normalised Vegetation Index) archive of SPOT/VEGETATION for the  
196 year 2000 at a 1km resolution. Using differences in the NDVI profiles, the crop classes  
197 of Corine were split into 20 subsets (referred as C1, C2, .. to C20 in the following). The  
198 distribution of these crop types within the main basins is presented figure 4. Among the  
199 large basins, the Seine basin is the most cultivated, with 60 % of the surface covered by  
200 crops. The Loire and Adour-Garonne basins have about the same crop surfaces (54 and  
201 51 %, respectively), whereas the Rhone basin is the least cultivated large basin (31%),  
202 primarily because the eastern part of the basin is mountainous.

203 The crop partition is different within each basin: the 2 dominant crop types represent  
204 half of the cultivated area of the Seine basin, while in the other basins, it represents only  
205 one fifth (figure 4) .

206 The 10-day NDVI cycles of the dominant crop types are presented in figure 5. The  
207 NDVI cycle cannot be used to directly identify the type of the crop class, however the  
208 class C7, which is dominant in the Adour-Garonne basin with a maximum NDVI from  
209 July to September, is representative of summer crops, especially Maize. In contrast, the  
210 C1 class, with a very narrow cycle, and which is mostly present in the North of France, is  
211 associated with winter crops, such as wheat, as well as the classes C8 and C9 dominant  
212 in the Seine and Loire basins.

213 In order to derive the ISBA vegetation parameters, the ECOCLIMAP correspondence  
214 tables were used. The annual LAI (leaf area index) cycle is based on the 10-day NDVI  
215 tendencies, with the extreme values of the LAI fixed for each vegetation type (from 0 to 4  
216  $m^2/m^2$  for crops). Then the 10-day evolution of the vegetation fraction, roughness length,  
217 and albedo are derived using the formulations given by Masson et al., 2003. For the other

218 vegetation types, the annual cycle was re-computed at a 10-day time step instead of the  
219 monthly time step used in the ECOCLIMAP global database.

220 The soil map used in the Ecoclimap France database is taken from the INRA 1km  
221 soil geographical database (Base de données géographique des Sols de France -BDGSF-  
222 [www.gissol.fr/programme/bdgsf/bdgsf.php](http://www.gissol.fr/programme/bdgsf/bdgsf.php)). Only the percentages of sand and clay are  
223 used to define the soil parameters for ISBA (Noilhan and Lacarrère, 1995).

### 3.3. Atmospheric database

224 Data from more than 1000 surface meteorological stations and more than 3500 daily  
225 raingages were analysed by the SAFRAN system. SAFRAN has been used to produce  
226 an atmospheric database at an hourly time step over the France domain, for the period  
227 starting in August 1995 and ending in July 2005. A detailed presentation and assessment  
228 of the 8 variables analysed by SAFRAN for the years 2001-2002 and 2004-2005 can be  
229 found in Quintana-Seguí et al., 2007. Therefore, only the main characteristics of the  
230 10-year precipitation database are presented here.

231 The mean annual precipitation over the 10-year period is shown figure 6. As can be  
232 expected, precipitation is abundant in the mountains, and also, along the Atlantic coast.  
233 The south-eastern border of the Massif Central experiences heavy rainfall primarily in the  
234 fall season which leads to significant annual precipitation totals.

235 The Seine and Loire basins in the North receive less precipitation (*802mm/year*  
236 and *835mm/year*, respectively) than the southern basins that are more mountainous  
237 (*944mm/year* and *1186mm/year* for the Garonne and Rhone basins, respectively). The  
238 year 2000-2001 is the wettest for all of the basins, and the year 2001-2002 is the driest for  
239 all basins except the Seine (encapsulated graphs in figure 6). Snowfall, is shown in the

240 top of the histogram in figure 6. It is a key component of the Rhone basin precipitation  
241 and comprises 29% of the total. Despite the presence of the Pyrenees mountain range,  
242 snowfall is less significant in the Adour-Garonne basin, where it represents only 5.7% of  
243 the total precipitation. It represents less than 3% in the two other basins.

244 The monthly cycle of precipitation presents a similar pattern for almost all the basins on  
245 average over the 10 years. Precipitation has two maxima in the year: one in winter, and  
246 one in spring (figure 7). The cycle is less pronounced for the northern basins, where the  
247 average rainfall ranges from 1.58 to 3.2 *mm/day* in March and November, respectively,  
248 than in the southern basins where it ranges from 2 to 5 *mm/day*.

#### 4. Evaluation of the hydrometeorological modelling

249 The 10-year integration of the SIM system was assessed using various data, either local  
250 or spatially integrated, and either instantaneous or averaged over a certain time period.  
251 This section presents the comparison of the simulation with the daily observed riverflows,  
252 the piezometric levels and the snow depths.

##### 4.1. Comparison with observed riverflow

253 Figure 8 presents the daily riverflows at the rivergages located closest to the outlet of the  
254 4 largest rivers of France which are not affected by the tide (the location of the rivergages  
255 can be seen figure 10). The observed riverflows are plotted using dark circles, and the  
256 simulation is represented by the continuous lines. The Garonne at Lamagistere has the  
257 smallest upstream area (50430  $km^2$ ), and logically has the lowest average discharge, but  
258 it has higher flood peaks than the Seine basin at Poses (wich has an upstream area of  
259 65686  $km^2$ ). This is due to the fact that the Garonne encompasses part of the Pyrennees

260 and Massif Central mountains, where heavy orographically enhanced precipitation can  
261 occur, while the Seine basin overlays a widespread aquifer, which tends to reduce the  
262 winter flood peaks and to sustain the summer low flow. The Loire at Montjean sur Loire,  
263 which has the largest upstream area ( $110356 \text{ km}^2$ ) has an average discharge almost two  
264 times lower than that of the Rhone at Beaucaire, which has a smaller contributive area  
265 ( $96412 \text{ km}^2$ ). This results because the Rhone basin encompasses part of several mountain  
266 ranges, notably the Alps. The Rhone rivers had 2 large flood events during the period  
267 under investigation, in December, 2002, and December, 2003. Unfortunately, observed  
268 discharge data have not been available at Beaucaire since 2003.

269 SIM is capable of representing the dynamic of the flows measured at these 4 rivergages.  
270 However, some deficiencies can be seen. For instance, SIM tends to underestimate the  
271 summerflow of the Rhone at Beaucaire. This is mainly due to the fact that the model  
272 does not take into account the numerous dams used for hydro-electricity power in the  
273 Alps which tend to sustain the summerflow. As for the Garonne and Loire rivers, the  
274 recession of the flood peaks are too fast in the model. This is partially due to the fact  
275 that the main water tables are not simulated in those 2 basins.

276 To quantify the ability of the SIM system to represent the daily riverflows, two statistical  
277 results are used: the discharge ratio ( $q_{sim}/q_{obs}$ ) and the efficiency,  $E$ , (Nash and Sutcliffe,  
278 1972). These statistical criteria were computed at a daily time scale over the full period  
279 with available observations. The SIM system is able to simulate the riverflows at the  
280 outlet of these 4 main basins with a good accuracy, corresponding to an efficiency ranging  
281 from 0.68 to 0.88, and an error on the discharge ranging from  $-10\%$  to  $+6\%$ .

282 Figure 9 presents the results obtained by SIM over 610 rivergages with available data,  
283 as a function of the surface of the rivergage basin. Each circle represents a rivergage, and  
284 the linear regression line is shown (it appears as an exponential, due to the log x-axis  
285 unit). Of course, there are more stations with a small area (below  $1000\text{km}^2$ ), than with  
286 a large area (above  $10000\text{ km}^2$ ). The index of agreement (Willmot, 1981) is above 0.8 for  
287 most of the rivergages, and there are few river gages with an index of agreement below  
288 0.6. In general, the bad results for these stations are due to the fact that either the river  
289 is influence significantly by dams (e.g. Durance and Isere rivers), or that they are have  
290 non-negligible interaction with a large aquifer that is not explicitly taken into account  
291 (e.g. Somme and Leyre rivers). There is a clear link between the quality of the simulation  
292 and the surface of the river basin: Figure 9 shows that the average efficiency is close  
293 to 0.5 for the small riverstations, while it is around 0.7 for the larger ones. Moreover,  
294 there is a larger ratio of rivergages with a very good efficiency (above 0.8) for the larger  
295 basins. There are several factors that lead to the overall better results for the large basins.  
296 One key point is that the forcing data has larger errors for small basins (essentially the  
297 precipitation). In the large basins, some errors in the upstream basin can be compensated  
298 for downstream, leading to overall better results. The same kind of compensation can  
299 occur for the description of the geological and surface properties. An additional reason  
300 could be that the human activities (dams, derivation, pumping, ...) can have relatively  
301 larger effect on the small basin discharge. Finally, larger errors may be due also to the  
302 faster hydrologic response of those basins which cannot be reproduced by the relatively  
303 simple river routing model used herein.



304 The encapsulated graph presents the histogram of the efficiency. The maximum of  
305 the histogram is reached for an efficiency between 0.6 and 0.7 (121 rivergages). 101  
306 rivergages have an efficiency above 0.7, and only 20 have values above 0.8. That implies  
307 that more than 36% of the rivergages was associated with a daily efficiency over the full  
308 period that can be considered as "rather good" ( $E > 0.6$ ), and 16% as "fair" ( $E > 0.7$ ).

309 Another 30 % of the rivergages have an efficiency that can be considered as reasonable  
310 ( $0.55 < E < 0.65$ ). There are 97 stations with an efficiency below 0 (very poor, not shown  
311 in figure 9), which represents 15% of the rivergages, and is comparable to the large scale  
312 study by Henriksen et al. (2003). This subset includes all of the rivergages which are  
313 significantly affected by dams.

314 The discharge error is close to zero on average, but is more scattered for the small  
315 basins than for the larger basins. The encapsulated histogram is centered on zero, which  
316 is consistent with the results of the regression fit.

317 Figures 10 and 11 present the spatial repartition of the efficiency and of the discharge  
318 ratio, with the results at each gage and their associated river network. As expected, the  
319 results are quite good for the main rivers. Nonetheless, some areas have poor results in  
320 terms of efficiency: notably the Alps and the Northern portion of the domain. For the  
321 Alps, this is mainly due to the fact that this region is used to produce hydropower, and the  
322 natural riverflows are perturbed by numerous dams. To a lesser extent, some of the water  
323 is also used for irrigation or drinking water. Similar results were also found in previous  
324 studies in the Rhone and Garonne basins (Etchevers et al., 2001a,b,2002, Habets et al.,  
325 1999, Morel 2003). In the upper mountains, there is relatively little water extraction, and  
326 most of the water is simply stored in reservoirs for hydropower. This is not the case in the

327 lower Durance, where a significant part of the water is diverted for irrigation and drinking  
328 water. It can be seen in figure 11 for the Alps that although the efficiency is poor, the  
329 discharge is well estimated with an error below 10%. Poor results in the two rivers in the  
330 northern part of France are due to the fact that a large aquifer which is closely connected  
331 to the rivers is not yet simulated by SIM. The discharge is underestimated in one of the  
332 2 rivers, and it is estimated quite well for the other one. Except for these 2 regions, the  
333 results are quite homogeneous over all of France.

334 As the simulated period covers contrasting climates, it is of interest to look at the time  
335 evolution of the statistical results. In order to be able to compare the statistics from  
336 year to year, it is essential to have a homogeneous set of rivergauge time series. Therefore,  
337 the rivergages with more than 200 days of observations available each year were selected.  
338 Moreover, in order to be able to aggregate the results, another criteria was added: the  
339 efficiency should be positive each year. There are 140 rivergages that fit these criteria.  
340 The corresponding results are presented in figure 12 for 5 large basins, and on average  
341 for all of France. The discharge ratio and the efficiency are shown, together with their  
342 regression fits which give the overall tendency. The statistical results vary from year to  
343 year. In addition, they also vary from one basin to the next, but, there are some common  
344 characteristics when looking at the efficiency: the best results are obtained in the year  
345 2002-2003, while the worst are found in one of the 3 following years: 1995-96 2001-02  
346 or 2004-05. The results are less homogeneous in terms of the discharge ratio. It tends  
347 to decrease during the entire time period for the Loire and Garonne basins, leading to a  
348 reduction of the error on the Loire, and to an increase on the Garonne. There is no clear  
349 signal in the Rhone and Seine basins. Over all of the France, there is a slight tendency

350 for the discharge ratio decrease, with an underestimation around 8% at the end of the  
351 period. In general, there is no clear relation between the efficiency and the error in the  
352 discharge of a given year. However, it appears that the model obtains worst results in  
353 terms of efficiency during the driest years. This is clearly seen in figure 13 where the  
354 observed annual discharge is shown along with the resulting efficiency on the average for  
355 each of the 5 basins and for all the selected stations. The difficulty with dry periods can  
356 have several explanations: i) the low flows are sustained by the various water tables, and  
357 only a few of them are explicitly represented in SIM ii) processes associated with dryness  
358 or low soil moisture are perhaps poorly simulated by the SIM model, and iii) part of the  
359 error is probably due to the human management of the river (not taken into account by  
360 SIM), since both the effect of the dams, and the pumping in rivers or from the watertables  
361 have more impact during the period of low flow. However, figure 13 shows that although  
362 the results tend to improve when the observed discharge increases, the best results are  
363 not obtained for the wettest year.

#### 4.2. Comparison with observed piezometric head

364 Piezometric head is thoroughly monitored in France, and numerous data are available.  
365 For the Seine basin, the piezometric gages were selected in order to keep only the rep-  
366 resentative ones, i.e., those that are not impacted by pumping, and those that are not  
367 too close to a river. Thus, 43 observation sites were chosen, with data available for the  
368 10 year study period. Such a selection was more difficult in the Rhone basin because  
369 the watertable is along the river: therefore only 8 gages were retained. The location of  
370 the selected piezometric gages as well as the average bias between the simulation and the  
371 observation of the piezometric head are shown in figure 14. There are some points where

372 the absolute bias is above 10m, especially for the Rhone basin. However there are 20  
373 gages for which the absolute bias is lower than 2m. One such gage is located in the Rhone  
374 basin, and the other ones are spread over the 3 aquifer layers of the Seine basin. Figure  
375 15 presents the comparison between observed and the simulated piezometric head for the  
376 4 gages encircled in figure 14. The amplitude of variation of the Rhone aquifer at Genas  
377 is rather weak, because the aquifer level is constrained by the river. For the Seine basin,  
378 the annual amplitude varies from gage to gage. However, for almost every gage, there is  
379 an increase of the piezometric head during the wet year 2000-2001, and a clear decrease  
380 in 2003-2004. These evolutions are well captured by the model.

#### 4.3. Comparison with the observed snow depth

381 The snow accumulation and melt are key components of the water and energy budgets.  
382 The comparison with observed and simulated snow depths is possible at some meteorologic  
383 observing stations and at numerous mountain sites. In order to be sure of the quality of the  
384 observed data set, only the stations that observed at least 30 days of non-zero snow depth  
385 during the 10-year period are selected. Moreover, the comparison between observations  
386 and the simulation are made only if the altitude of the grid cell is close to that of the  
387 station (less than 150m difference). With this selection criteria, 505 stations with snow  
388 depth measurements were selected. As the snow cover depends mostly on the altitude  
389 in France, figure 16 presents the daily comparison between observed and simulated snow  
390 depths for altitude bands. The number of station varies for each level from 19 for the  
391 upper level (above 2000m) to 179 for the level 250-750m. However, the observations are  
392 not available each day at all stations, so that the number of stations used to compute  
393 the average varies from day to day (with a minimum of 2 stations). As expected, the

394 snowpack generally lasts longer and is deeper as the altitude increases. The snowpack  
395 has large interannual variations which vary at each level. However, the plotted evolution  
396 is affected by the number of gages used to compute the average which vary each day. In  
397 order to be able to estimate the temporal evolution of the snow pack, the snow depth  
398 simulated by SIM on average for all the stations selected for each level is presented in  
399 the bottom left panel of figure 16. In this figure, the same number of points are used  
400 everyday, thus leading to a real temporal evolution. The bias and the squared correlation  
401 between observation and simulation are given in figure 16. The model is able to reproduce  
402 the observed evolution of the snowpack. The bias is rather low on average (around  $3cm$   
403 up to  $10cm$  at the highest level), even if the error can be large at times. The squared  
404 correlation is low for the lowest level where the snowpack does not last long, and reaches  
405 0.7 at the highest level. Figure 17 presents about the same data set, but on an annual  
406 basis. The annual evolution of the snow pack is well estimated by the model, with the  
407 squared correlation which reaches 0.9 for all levels except the lowest one. However, there  
408 are systematic errors in the two highest levels: an underestimation of the snow depth from  
409 January to February for the level 1250m-2000m, and, in contrast an overestimation of the  
410 snow depth from September to January for the level above 2000m, and during the melting  
411 period in May-June. It is difficult to estimate how such systematic error may affect the  
412 water budget and the simulation of the streamflows, since those results are affected by  
413 the availability of the observations. For instance, it can be seen on the lower right panel  
414 that the maximum snow depth is simulated in February, whereas it appears to be in early  
415 May in the comparison with the observations for the upper level.

#### 4.4. Water and energy budgets at the basin scale

416 The simulated annual water and energy budgets can be partially assessed using the  
417 comparison between observed and simulated discharges. For that, there is a focus only on  
418 the largest subbasins, using the rivergages with the longest observation periods. Figure 18  
419 presents the results for the 4 main basins (Rhône at Beaucaire, Seine at Paris, Garonne  
420 at Tonneins and Loire at Nantes). For these basins, the discharge error for the whole  
421 period represents +63, +24, -15 and +50  $m^3/s$ , which corresponds to an average error in  
422  $mm/year$  of +26,+18,-10,+14, respectively (see Table 1). The error for the Rhône basin  
423 is the largest. This is due in part to the large anthropogenic impact, which consists in  
424 numerous dams and canals in the Durance and Isère river basins. For instance, in 2003  
425 in the Durance subbasin, the total quantity of water derived to sustain human activities  
426 (irrigation, drinking water, cooling of energy plants, ...) was  $37m^3/s$ , which represents  
427 approximately half of the error at Beaucaire for this single subbasin (data available on  
428 the web site [www.rhone-mediterranee.eaufrance.fr/telechargement/index.php](http://www.rhone-mediterranee.eaufrance.fr/telechargement/index.php)). However,  
429 it is difficult to estimate which part of this water is going back to the river network.

430 A simple estimation of the evaporation error at the basin scale can be made by assuming  
431 that all of the discharge error only results from evaporation. This implies several strong  
432 hypotheses: i) there is no error in the precipitation at the basin scale, ii) there is no error  
433 in the observations of the riverflow iii) there is no error in terms of the estimation of the  
434 water storage in the soil, the snowpack, the aquifers and the rivers at the annual scale,  
435 and iv) the water storage in the dams is not significant on a annual scale. Using this  
436 estimated error, it is possible to analyse the spatial and temporal evolution of the water  
437 and energy budgets.

438 The annual evaporation is quite similar for the 4 bassins, ranging from  $573\text{ mm/year}$  on  
439 average for the Seine basin to  $634\text{ mm/year}$  on average for the Garonne, with an annual  
440 amplitude of about  $\pm 100\text{ mm/year}$  (which is quite smooth over the 10-year period: table  
441 1). On average over the 10-year period, the estimated evaporation error represents about  
442 4% of the annual flux. However it varies from year to year, and can reach 8% of the  
443 annual evaporation and even 15% in the Rhone basin in 2000-2001 (table 1). The Rhone  
444 basin is the only large basin for which the total runoff is about the same magnitude as  
445 the evaporation (about  $590\text{ mm/year}$ ). For the other basins, the total runoff is about two  
446 times lower than the evaporation. The evolution of the annual runoff is less smooth than  
447 the annual evaporation and more closely follows the annual variation of the precipitation.

448 In terms of the energy budget, only the latent heat flux error can be estimated, and one  
449 cannot determine how this error affects the sensible, ground heat and the net radiation  
450 fluxes. Thus, the estimated latent heat flux error is presented independently of the other  
451 energy budget terms. This error, expressed in  $W/m^2$ , varies from  $-0.8W/m^2$  in the  
452 Garonne basin to  $1.7W/m^2$  in the Rhone basin. It is striking that the error estimated on  
453 the latent heat flux roughly accounts for 10% of the sensible heat flux, and that they are  
454 of the same order of magnitude in the Rhone basin in 2000-2001. Indeed, the averaged  
455 annual sensible heat flux ranges between  $15.3W/m^2$  in the Rhone basin to  $19W/m^2$  in the  
456 Loire basin. Its annual evolution can be rather smooth as in the Rhone basin (from 10  
457 to  $20\text{ W/m}^2$ ) or more pronounced as in the Seine basin (from 6 to  $30\text{ W/m}^2$ ). The net  
458 radiation is 10 % larger in the Garonne basin than in the Seine or Rhone basins. But for  
459 all of the basins, the annual evolution of the net radiation is quite smooth, with a total  
460 amplitude of  $\pm 6\%$ .

461 Figure 19 shows maps of the Bowen ratio and the ratio of the evaporation to precipi-  
462 tation. The two maps show large contrasts over France. The largest value of the Bowen  
463 ratio are along the southern Alps (where the snowfall is significant, thus limiting the  
464 evaporation, but where the incoming radiation fluxes are large), along the Mediterranean  
465 coast (including Corsica), and for two areas along the west coast. Half of the areas where  
466 the Bowen ratio is above 0.75 correspond to areas where the average annual rainfall is  
467 below  $650\text{mm}/\text{year}$  or where the net radiation is above  $80\text{W}/\text{m}^2$ . The residual is mostly  
468 located in Corsica and along the eastern Mediterranean coast, and corresponds to the  
469 regions where the precipitation can be intense. Here, relatively few rain events produce  
470 large amounts of precipitation primarily during the fall season, and they produce large  
471 proportion of runoff, thereby reducing the evaporation rate. This is also the reason why  
472 the evaporation in this Mediterranean region represents less than 75% of the precipita-  
473 tion, even in areas where the precipitation is lower than  $650\text{ mm}/\text{year}$ , as is the case for  
474 instance in the "Bouches du Rhone" site indicated in figure 19. In contrast, the area in  
475 the Vienne department (cf flag on the maps) has both a large value of the Bowen ratio and  
476 of the ratio of the evaporation to precipitation. The other areas, where at least 75 % of  
477 the precipitation evaporates, are located around the Seine basin and the Garonne Valley.  
478 Such results are consistent with those obtained by Rousset et al., (2004) and Voirin-Morel  
479 (2003), respectively, for different time periods than examined in the current study.

480 Figure 20 shows the time evolution of the soil wetness index for the 3 points indicated  
481 in figure 19. In addition to the sites in the Vienne and Bouches du Rhone departments,  
482 one site in the Creuse department was selected as being representative of a weak Bowen  
483 ratio and an average  $E/P$  ratio . The 10-year average value of the fluxes for these



484 3 sites are given in table 2. The soil wetness index is computed from the expression  
485  $SWI = (w_{tot} - w_{wilt}) / (w_{fc} - w_{wilt})$ , where  $w_{tot}$  is the volumetric water content of the  
486 simulated soil column,  $w_{fc}$  is the field capacity, and  $w_{wilt}$  the wilting point. Thus, a value  
487 of the soil wetness index above 1 indicates that there is no evaporative water stress, and a  
488 value of 0 indicates that plant transpiration has ceased. At Creuse site the minimum value  
489 of the SWI in summer is the highest (just below 0.25 in 2003 and close to 0.5 in 1997),  
490 which indicates a moderate water stress for the vegetation. On the other hand, the water  
491 stress is significant in summer at the Bouches du Rhone site, with a SWI below 0.1 during  
492 4 years out of 10, and a minimal value below 0.02 reached during the exceptionally hot  
493 and dry summer of 2003. At the Vienne site, the summer value of the SWI is around 0.17,  
494 with a minimum value of 0.12 in 2005 after a dry winter. In winter time, the maximum  
495 value of the SWI is below 1, meaning that there is a water stress in winter 5 years out of  
496 10 in the Bouches du Rhone site, and 2 years out of 10 in the Vienne site. Such a pattern  
497 does not occur at the Creuse site.

498 The encapsulated graph in figure 20 represents the mean annual evolution of the soil  
499 moisture. The Creuse and Vienne sites have similar temporal evolutions, with a drier  
500 soil at Vienne (0.55 on average) compare to Creuse (0.75 on average). The temporal  
501 evolution of the SWI is slightly shifted in the Bouches du Rhone site, with an increase  
502 of the SWI starting early September due to significant precipitation, and the maximum  
503 value is reached in November, with a 10-year average value of 0.5.

504 Another interesting result which can be obtained with the SIM system is the evaluation  
505 of the total volume of the water that reaches the Mediterranean sea, via the large rivers  
506 but also the smallest. This is of interest since this component of the water budget of

507 the Mediterranean sea is not well-known. The simulated hydrographic network takes into  
508 account 80 rivers that flow to the Mediterranean Sea (30 are located in Corsica), and  
509 only 30 of them have a basin larger than  $250 \text{ km}^2$ . According to the simulation, 2287  
510  $\text{m}^3/\text{s}$  flows to the Mediterranean sea on average every year. 80% of this flow is from the  
511 Rhone river, and 91% by the 10 largest Mediterranean rivers (2 being located in Corsica).  
512 Most of those Mediterranean rivers are located in mountainous regions, characterised by  
513 a significant snow cover in winter, leading to a smaller fraction of the precipitation that  
514 evaporates (55% on average).

## 5. Conclusion

515 The hydrometeorological model SAFRAN-ISBA-MODCOU (SIM) was extended to all  
516 of France in order to have a homogeneous estimation nationwide of the water resource.  
517 The 10-year simulation was compared with daily riverflow, piezometric head, and snow  
518 depth observations. SIM obtained reasonable results (efficiency above 0.55) for more than  
519 66 % of the 610 rivergages simulated, and rather good results (efficiency above 0.65) for  
520 more than 36 % of them. It was found that worse results were obtained during the driest  
521 years, which is more likely due to the fact that only few aquifers are simulated explicitly.

522 These comparisons show that SIM is quite robust both in space and time, and gives  
523 a good estimation of the water fluxes. As the ISBA surface scheme is used in weather  
524 forecast and climate models, it is important to estimate the quality of the simulated latent  
525 heat flux. The comparison with the observed riverflow, associated with some hypotheses,  
526 permits an estimation that the error is less than 4% on annual average.

527 Since 2003, the SIM system has been used operationally at Meteo-France: for each D,  
528 it performs an atmospheric analysis and hydrological simulation of day D-1. It is the first

529 time that such a system is used to monitor the water budget of France in real time, and  
530 especially, to estimate the soil wetness. The soil wetness can be used to estimate the flood  
531 risk, or to monitor the spatial and temporal evolution of a drought. Such information  
532 is now part of the national hydrological bulletin of the French environment ministry  
533 ([www.eaufrance.fr](http://www.eaufrance.fr)), which is published monthly.

534 The SIM operational application is also used to prescribe the initial condition for an  
535 ensemble riverflow forecasts system over all of France. The 10-day ensemble precipita-  
536 tion forecast are taken from the European Centre for Medium-Range Weather Forecasts  
537 (ECMWF), and then disaggregated in space. They are then employed as an input for the  
538 ISBA-MODCOU hydrometeorological system to make 10-day forecasts of the riverflows  
539 (Rousset et al., 2006 Rousset et al., 2007).

540 As in the NLDAS and CALDAS projects (Mitchell et al., 2004, Balsamo et al., 2006),  
541 the operational hydrometeorological model SIM can also be used to prescribe the initial  
542 soil moisture conditions of a mesoscale weather model. Some first attempts have been  
543 made with the Meso-NH mesoscale model (Donier et al., 2003) and such an approach  
544 could be generalised in the near future.

545 It is planned to increase the period of time covered by the SIM system in order to be able  
546 to use it for climatological and statistical analyses. For instance, in the Seine basin, 18  
547 years of the SAFRAN analysis were used with the ISBA-MODCOU hydrometeorological  
548 model in studies by Boé et al. (2006) and Boé et al. (2007) in order to disaggregate in  
549 space and time the simulation of a climate model. It was also used estimate the ability  
550 of this climate model to reproduce the observed present day conditions.

551 **Acknowledgments.** We would like to thank the French National Program for the  
552 Research in Hydrology (PNRH) for its financial support in this action.

## References

553 Artinyan, E., F. Habets, J. Noilhan, E. Ledoux, D. Dimitrov, E. Martin, P. Le  
554 Moigne, (2007), Modelling the water budget and the riverflows of the Maritsa basin  
555 in Bulgaria, submitted to *Hydrology and Earth System Sciences*, available online  
556 [www.copernicus.org/EGU/hess/hessd/4/475/hessd-4-475.pdf](http://www.copernicus.org/EGU/hess/hessd/4/475/hessd-4-475.pdf)

557 Balsamo, G., JF. Mahfouf, S. Bélair and G. Deblonde, (2007), A global root-zone soil  
558 moisture analysis using simulated L-band brightness temperature in preparation for the  
559 Hydros satellite mission. *J of Hydromet.*, to appear

560 Benoit, R, P. Pellerin, N. Kouwen, H. Ritchie, N. Donaldson, P. Joe, and E.D. Soulis  
561 (2000) Toward the use of coupled atmospheric and hydrologic models at regional scale,  
562 *Mon. Wea. Rev.*, *128*, 1681-1706

563 Boé, J. L. Terray, F. Habets and E. Martin (2006), A simple statistical-dynamical down-  
564 scaling scheme based on weather types and conditionnal resampling, *J. Geophys. Res.*,  
565 *111*, D23106.

566 Boé, J. L. Terray, F. Habets and E. Martin (2007), Statistical and dynamical downscaling  
567 of the Seine basin climate for hydro-meteorological studies, *International Journal of*  
568 *Climatology*, accepted

569 Boone, A., J. C. Calvet and J. Noilhan (1999), Inclusion of a third soil layer in a land  
570 surface scheme using the force-restore method, *J.Appl.Meteorol.*, *38*, 1611-1630.

571 Boone, A. and P. Etchevers (2001), An inter-comparison of three snow schemes of varying  
572 complexity coupled to the same land-surface model: Local scale evaluation at an Alpine  
573 site, *J.Hydrometeorol.*, 2, 374-394.

574 Boone, A., Habets F., Noilhan J., Clark D., Dirmeyer P., Fox S., Gusev Y., Haddeland I.,  
575 Koster R., Lohmann D., Mahanama S., Mitchell K., Nasonova O., Niu G. Y., Pitman  
576 A., Polcher J., Shmakin A. B., Tanaka K., Van den Hurk B., Verant S., Verseghy  
577 D., Viterbo P., and Yang Z. L., (2004), The Rhone-aggregation land surface scheme  
578 intercomparison project: An overview, *J.Clim.* 17, (1), 187-208.

579 Caballero, Y., S. Morel, F. Habets, J. Noilhan, P. LeMoigne, A. Lehenaff, A. Boone,  
580 (2007), Hydrological sensitivity of the Adour-Garonne river basin to climate change,  
581 *Water Res. Res.* In press doi:10.1029/2005WR004192

582 Chen, F., Z. Janjic and K. Mitchell (1997), Impact of atmospheric surface layer parame-  
583 terizations in the new land-surface scheme of the NCEP mesoscale Eta model, *Boundary*  
584 *Layer Meteorol.* 85, 391-421.

585 Donier S., F. Habets, P. Lacarrie, P. Le Moigne, J. Noilhan (2003) Initialisation of soil  
586 moisture in mesoscale atmospheric model *Geophysical Research Abstracts*, Vol.5 05467

587 Durand, Y., E. Brun, L. Merindol, G. Guyomarc'h, B. Lesaffre and E. Martin (1993), A  
588 meteorological estimation of relevant parameters for snow models, *Annales Geophysicae*,  
589 18, 65-71.

590 Etchevers, P., Y. Durand and F. Habets, E. Martin and J. Noilhan (2001), Impact of  
591 spatial resolution on the hydrological simulation of the Durance high-Alpine catchment,  
592 France *A. Glaciol.*, 32, 87-92.

593 Etchevers, P., C. Golaz and F. Habets (2001), Simulation of the water budget and the  
594 river flows of the Rhone basin from 1981 to 1994, *J. Hydrol.*, *244*, 60-85.

595 Etchevers, P., C. Golaz, F. Habets and J. Noilhan (2002), Impact of a climate  
596 change on the Rhone river catchment hydrology, *J. Geophys. Res.*, *107* (D16) , doi:  
597 10.1029/2001JD000490.

598 Golaz-Cavazzi, C., P. Etchevers, F. Habets, E. Ledoux, and J. Noilhan, (2001), Compar-  
599 ison of two hydrological simulations of the Rhone basin, *Physics and Chemistry of the*  
600 *Earth Part B*, *26*, iss. 5-6, p. 461-466.

601 Gomez, E., E. Ledoux, P. Viennot, C. Mignolet, M. Benoit, C. Bornerand, C. Schott B.  
602 Mary, G. Billen, A. Ducharne and D. Brunstein (2003), An integrated modelling tool  
603 for nitrates transport in a hydrological system: Application to the river Seine Basin, *La*  
604 *Houille Blanche*, *3*-2003, 38-45.

605 Habets, F., P. Etchevers, C. Golaz, E. Leblois, E. Ledoux, E. Martin, J. Noilhan and C.  
606 Otle (1999a), Simulation of the water budget and the river flows of the Rhone basin,  
607 *J. Geophys. Res.*, *104*, 31145-31172.

608 Habets, F., J. Noilhan, C. Golaz, J. P. Goutorbe, P. Lacarrere, E. Leblois, E. Ledoux, E.  
609 Martin, C. Otle and D. Vidal-Madjar (1999b), The Isba surface scheme in a macroscale  
610 hydrological model applied to the Hapex-Mobilhy area. Part I: Model and database, *J.*  
611 *Hydrol.*, *217*, 75-96.

612 Habets, F., J. Noilhan, C. Golaz, J. P. Goutorbe, P. Lacarrere, E. Leblois, E. Ledoux, E.  
613 Martin, C. Otle and D. Vidal-Madjar (1999c), The Isba surface scheme in a macroscale  
614 hydrological model applied to the Hapex-Mobilhy area. Part I: Simulation of streamflows  
615 and annual water budget, *J. Hydrol.*, *217*, 97-118.

616 Henriksen H., Troldborg L., Nyegaard P., Sonnenborg T., Refsgaard J., Madsen B. (2003),  
617 Methodology for construction, calibration and validation of a national hydrological  
618 model for Denmark, *J. Hydrol.*, 280, 52-71

619 Ivanov, V.Y, E.R Vivoni, R.L. Bras and D. Entekhabi (2004), Catchment hydrologic  
620 response with a fully distributed triangulated irregular network model. *Water Resour.*  
621 *Res.* 40, W1102, doi:10.1029/2004WRR003218.

622 Ledoux, E., G. Girard, G. De Marsily and J. Deschenes (1989), Spatially distributed  
623 modeling: Conceptual approach, coupling surface water and ground-water, in *Unsat-*  
624 *rated flow hydrologic modeling: theory and practice*, edited by H. J. Morel-Seytoux, pp.  
625 435-454, NATO Sciences Service.

626 Liang, X., D.P. Lettenmaier, E.F. Wood, S.J. Burges (1994), A simple hydrologically based  
627 model of land surface water and energy fluxes for general circulation models. *J. Geophys.*  
628 *Res.* 99 (D7) 14,415-14,48

629 Masson, V., J. L. Champeaux, F. Chauvin, C. Meriguet and R. Lacaze (2003), A global  
630 database of land surface parameters at 1 km resolution in meteorological and climate  
631 models, *J. Clim.*, 16, 1261-1282.

632 Mitchell, K. E., D. Lohmann, P. R. Houser, E. F. Wood, J. C. Schaake, A. Robock, B.  
633 A. Cosgrove, J. Sheffield, Q. Duan, L. Luo, R. W. Higgins, R. T. Pinker, J. D. Tarpley,  
634 D. P. Lettenmaier, C. H. Marshall, J. K. Entin, M. Pan, W. Shi, V. Koren, J. Meng,  
635 B. H. Ramsay, and A. A. Bailey, (2004), The multi-institution north american land  
636 data assimilation system (nldas): Utilizing multiple gcip products and partners in a  
637 continental distributed hydrological modeling system. *J. Geophys. Res.*, 109 D07S90,  
638 doi:10.1029/2003JD003823.

639 Miller, J.R., L.G. Russel and G. Caliri (1994), Continental scale river flow in climate  
640 models, *Journal of Climate*, 7, 914-928

641 Nash, J. E. and J. V. Sutcliffe (1970), River flow forecasting through conceptual models,  
642 *J. Hydrol.*, 10(3), 282-290.

643 Noilhan, J. and P. Lacarrère (1995), GCM gridscale evaporation from mesoscale modeling  
644 *J. Climate*, 8(2), 206-223.

645 Noilhan, J. and J-F. Mahfouf (1996), The ISBA land surface parameterization scheme,  
646 *Global Planet. Change*, 13, 145-159.

647 Noilhan, J. and S. Planton (1989), A simple parameterization of Land Surface Processes  
648 for meteorological Models, *Mon. Weather Rev.*, 117, 536-549.

649 Reed, S., V. Koren, M. Smith Z. Zhang F. Moreda, D-J. Seo (2004), Overall distributed  
650 model intercomparison project results. *J. of Hydrol.*, 298, 27-60

651 Ritter, B. and J. F. Geleyn (1992) A comprehensive radiation scheme for numerical  
652 weather prediction models with potential applications in climate simulations. *Monthly*  
653 *Weather Review*, 120, 303-325.

654 Rousset, F., F. Habets, E. Gomez, P. LeMoigne, S. Voirin-Morel, J. Noilhan and E.  
655 Ledoux (2004), Hydrometeorological modeling of the Seine basin using hte SAFRAN-  
656 ISBA - MODCOU system, *J. Geophys. Res.*, 109, doi:10.1029 /2003JD004403.

657 Rousset-Regimbeau, F., F. Habets, E. Martin, 2006 Ensemble streamflow forecast over  
658 the entire France *Geophysical Research Abstracts*, Vol.8 01962

659 Rousset-Regimbeau, F., F. Habets, E. Martin, J. Noilhan (2007) Ensemble stream-  
660 flow forecasts over France *ECMWF Newsletter*, 111 21-27 (available online:  
661 [www.ecmwf.int/publications/newsletters/pdf/111.pdf](http://www.ecmwf.int/publications/newsletters/pdf/111.pdf))



662 Van der Hurk et al. 2005, ELDAS Final Report December 2001- December 2004, available  
663 in [www.knmi.nl/samenw/eldas/](http://www.knmi.nl/samenw/eldas/)

664 Voirin-Morel, S. (2003), Modélisation distribuée des flux d'eau et d'énergie et des  
665 débits à l'échelle régionale du bassin Adour Garonne, PhD Thesis, 292 pp, Univer-  
666 sité Paul Sabatier - Toulouse III, Toulouse, France. (<http://www.cig.enscm.fr/hydro/THE/the.htm>)

668 Quintana Seguí, P, P. Le Moigne, Y. Durand, E. Martin, F. Habets, M. Baillon, L.  
669 Franchisteguy, S. Morel and J.Noilhan, (2007), The SAFRAN atmospheric analysis.  
670 Description and Validation. *Journal of Applied Meteorology and Climatology* Accepted

671 Willmot, C. J. (1981), On the validation of models, *Phys. Geog.*, 2, 184-194.

672 Wood, E. F., et al. (1998), The Project for Intercomparison of Land-Surface Parame-  
673 terization Scheme (PILPS) Phase-2(c) Red-Arkansas river experiment: I. Experiment  
674 description and summary intercomparisons, *Global Planet. Change*, 19, 115-135.

## 6. figures

675 Figure 1: The SIM hydrometeorological model consists in of three independant modules:  
676 the SAFRAN atmospherical analysis, the ISBA land surface model, and the MODCOU  
677 hydrogeological model

678 Figure 2: Topography and hydrographic network

679 Figure 3: Simulated aquifers (cells) and main aquifers as defined in the BDRHF (Base  
680 de Données sur le Référentiel Hydrogéologique Français; <http://sandre.eaufrance.fr>) hydro-  
681 geological database (dashed)

682 Figure 4: The main types of vegetation from the ecoclimap-france data base

683 Figure 5: The 10-day evolution of the NDVI for the main crop types

684 Figure 6: Mean annual precipitation in mm/year. The encapsulated graph presents the  
685 annual precipitation for each year on average over the selected basin

686 Figure 7: Mean monthly precipitation averaged on the main basin

687 Figure 8: Daily observed (black circle) and simulated (line) riverflows at the outlet of  
688 the four main rivers. The scale vary for each gage. The title includes the mean observed  
689 discharge on the period  $Q_{obs}$ , the discharge ratio  $Q_{sim}/Q_{obs}$  and the efficiency  $E$ .

690 Figure 9: Efficiency (top), discharge error (middle), and index of agreement (bottom)  
691 for each simulated rivergages plotted versus the upstream area of the rivergages. The  
692 circles represent the rivergages, and the line is the linear regression (x-axis is log). The  
693 encapsulated graphs represent the histogramm of the statistical results.

694 Figure 10: Spatial representation of the efficiency for each rivergage and the correspond-  
695 ing river network.

696 Figure 11: Spatial representation of the discharge ratio for each rivergages and the  
697 corresponding river network.

698 Figure 12: Evolution of the efficiency (circles) and discharge ratio (squares) on average  
699 on 5 large basins and on average for all of France. Only the rivergages with more than  
700 200 days available each year (and with positive values of the efficiency) were taken into  
701 account. Their number is indicated on the plots

702 Figure 13: Relation between the efficiency and the observed discharge on average on  
703 the selected rivergages of each basin. The line correspond to the linear regression for a  
704 given basin

705 Figure 14: Spatial distribution of the bias on the 10-year simulation of the piezometric  
706 head simulated by SIM

707 Figure 15: Evolution of the observed (symbol) and simulated (line) piezometric head  
708 for one given station over each layer of the Seine and Rhone aquifers

709 Figure 16: Snow depth observed (black dots) and simulated (crosses) average on several  
710 gages according to their altitude (the average is computed each day on the stations with  
711 available data). The bottom right panel presents the evolution of the simulated snow  
712 depth on the selected stations of the 4 levels (the same number of stations is used each  
713 day to compute the average). Levels 750-1250m : black thick line; 1250-2000 gray line;  
714 over 2000m thin black line. The square correlation ( $R^2$ ) and the bias in cm (B) are given  
715 in the subtitle

716 Figure 17: Same as previous figure but on average on an annual cycle

717 Figure 18: Water and energy budgets over the 4 main basins. The thick black line is  
718 the total precipitation (Precip), and its thickness represents the snowfall. Evaporation  
719 (Evap), total runoff (Runoff) and latent heat flux (LEW) have an error bar that was  
720 estimated according to the error between the observed and simulated discharge. This  
721 error is shown in the energy budget panel (bottom panel) (Err) in order to compare  
722 with the net radiation (RN) and the sensible heat flux (H).

723 Figure 19: 10-year average bowen ratio ( $H/LE$ ) (left) and 10-year average ratio of the  
724 evaporation to precipitation (right).

725 Figure 20: 10-day evolution of the soil water index (SWI) on the 3 sites plotted in figure  
726 19. The encapsulated graph is the annual average

## 7. tables

727 table 1: Main characteristics of the water budget of the 4 main basins: E: mean annual  
728 evaporation, RO: mean annual total runoff, Err: averaged 10 years annual error computed

Table 1. Main characteristics of the water budget of the 4 main basins: E: mean annual evaporation, RO: mean annual total runoff, Err: averaged 10 years annual error computed with the observed riverflow (in mm/year and in  $W/m^2$ ), Err/E: percentage of the error compared to the mean annual evaporation, max Err: maximal annual error on the 10 years period, estimated with the observed riverflow, max Err/E: percentage of this maximal error compared to the annual evaporation of the year, year max: year where the error is maximal, RN: Net radiation, H: sensible heat flux, LE: latent heat flux.

Basin	Rhone Beaucaire	Seine Paris	Garonne Tonneins	Loire Nantes
Surface ( $km^2$ )	96412	43509	50430	112187
P ( $mm/year$ )	1189	820	956	834
E ( $mm/year$ )	590	573	634	574
RO ( $mm/year$ )	599	243	324	259
Err ( $mm/year$ )	26	18	-10	14
Err/E	4.4%	3.1%	1.6%	2.4 %
max annual Err ( $mm/year$ )	92	42	-51	49
max annual Err/E %	15%	8%	-9%	8%
year max annual error	2000-2001	2003-2004	2004-2005	2000-2001
Err ( $W/m^2$ )	1.7	1.5	-0.8	1.1
RN ( $W/m^2$ )	63.0	61.8	68.7	64.5
H ( $W/m^2$ )	15.3	16.4	18.4	19.1
LE ( $W/m^2$ )	46.9	45.6	50.3	45.6

729 with the observed riverflow (in mm/year and in  $W/m^2$ ), Err/E: percentage of the error  
730 compared to the mean annual evaporation, max Err: maximal annual error on the 10 years  
731 period, estimated with the observed riverflow, max Err/E: percentage of this maximal  
732 error compared to the annual evaporation of the year, year max: year where the error is  
733 maximal, RN: Net radiation, H: sensible heat flux, LE: latent heat flux.

734 table 2: Mean annual water and energy budget on the 3 gridcells indicated in figure  
735 19 Precip: total precipitation, Evap: evapotranspiration, H: sensible heat flux, LE: latent  
736 heat flux (same as Evap, but expressed in  $W/m^2$ ), RN: Net radiation, E/P: ratio of the  
737 evaporation over the precipitation, H/LE: Bowen ratio

Table 2. Mean annual water and energy budget on the 3 gridcells indicated in figure 19 Precip: total precipitation, Evap: evapotranspiration, H: sensible heat flux, LE: latent heat flux (same as Evap, but expressed in  $W/m^2$ ), RN: Net radiation, E/P: ratio of the evaporation over the precipitation, H/LE: Bowen ratio

Site	Precip mm/year	Evap mm/year	H $W/m^2$	LE $W/m^2$	RN $W/m^2$	E/P	H/LE
Vienne	637	507	34	40	76	0.80	0.88
Bouches du Rhone	650	428	29	34	63	0.65	0.86
Creuse	1167	675	12	53	65	0.58	0.22

738 1) un peu de texte

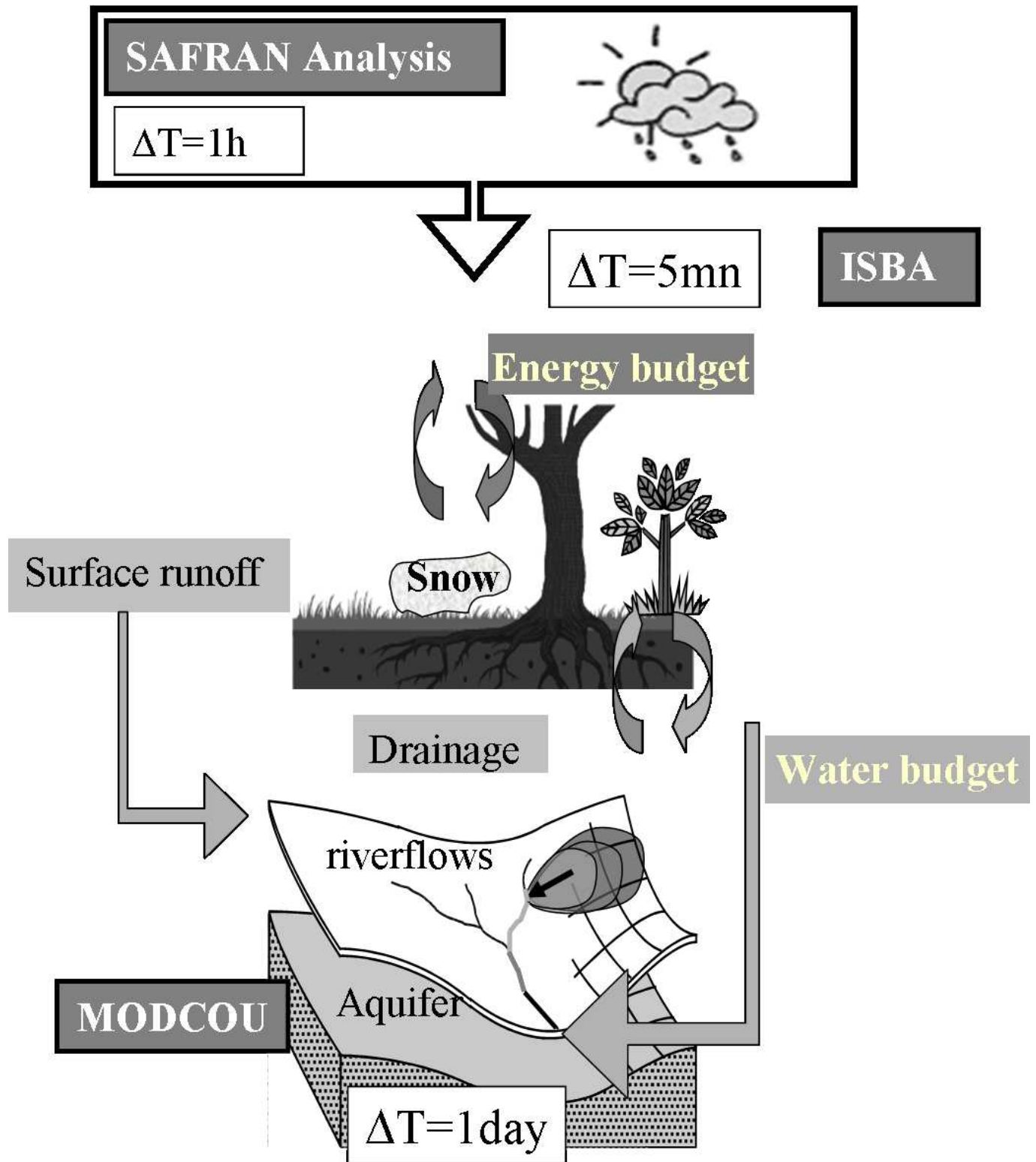


Figure 1. The SIM hydrometeorological model consists in three independent modules: the SAFRAN atmospheric analysis, the ISBA land surface model, and the MODCOU hydrogeological model

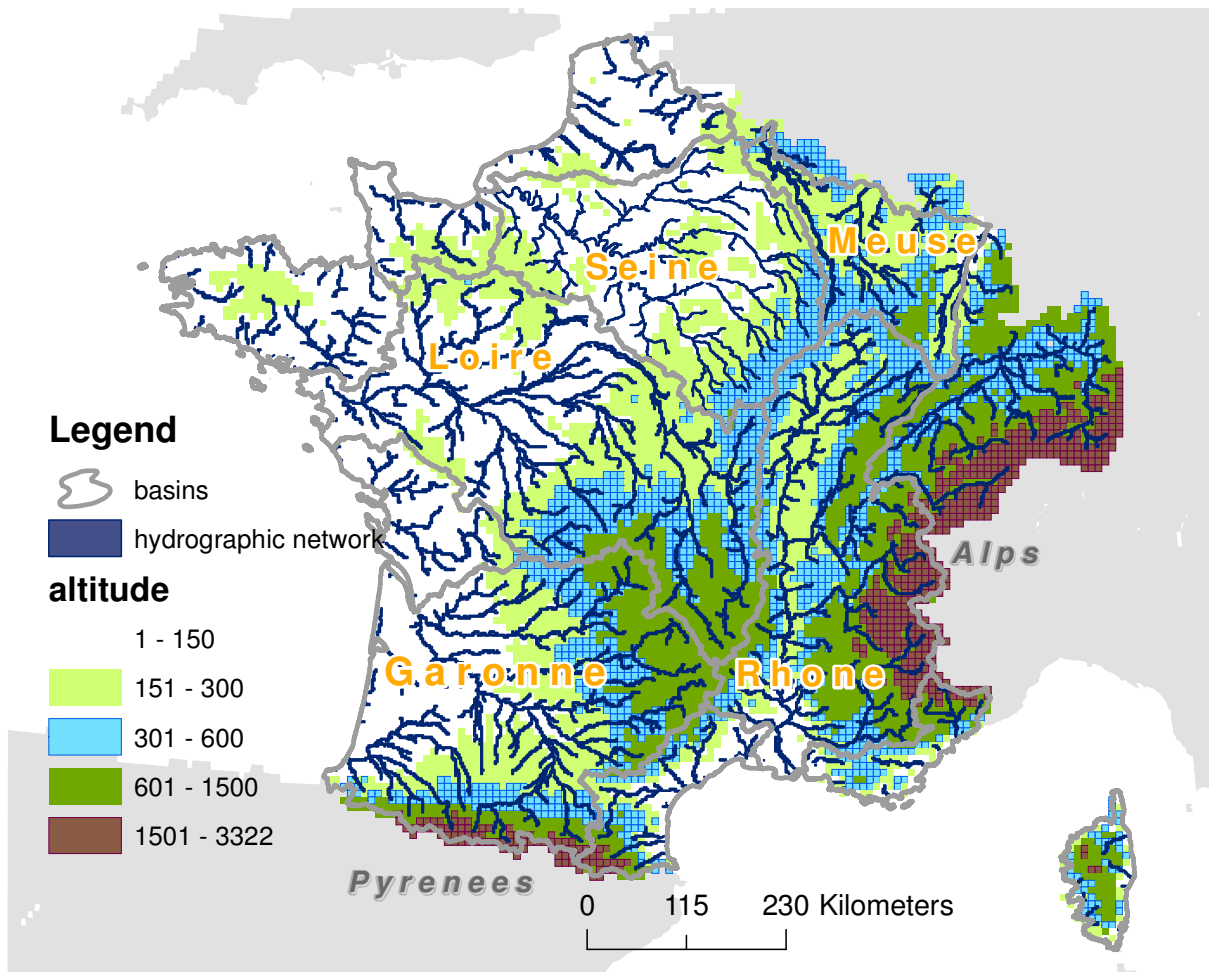


Figure 2. Topography and hydrographic network

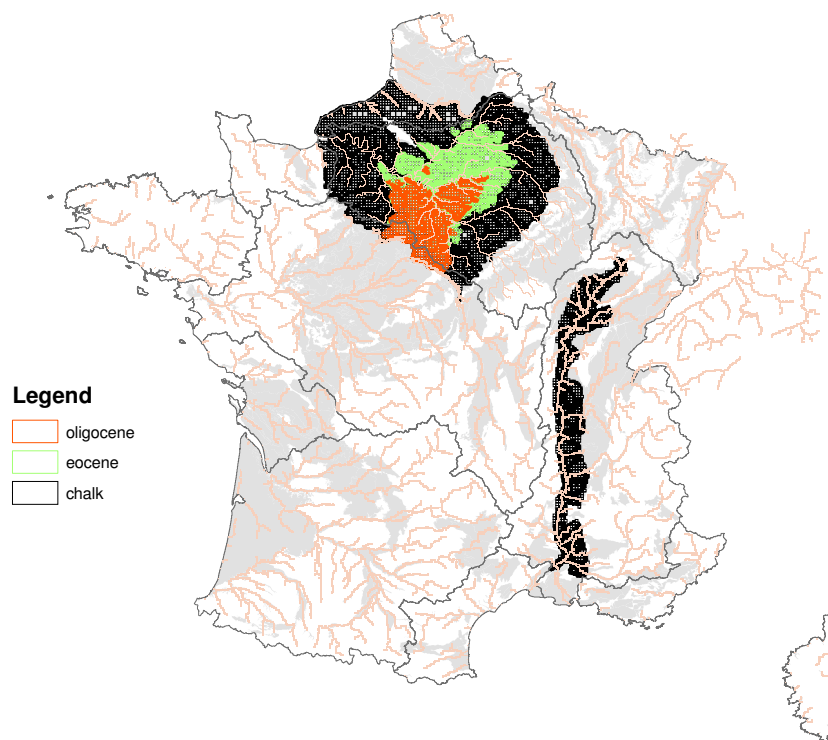


Figure 3. Simulated aquifers (cells) and main aquifers as defined in the BDRHF (Base de Données sur le Référentiel Hydrogéologique Français; <http://sandre.eaufrance.fr>) hydrogeological database (dashed)



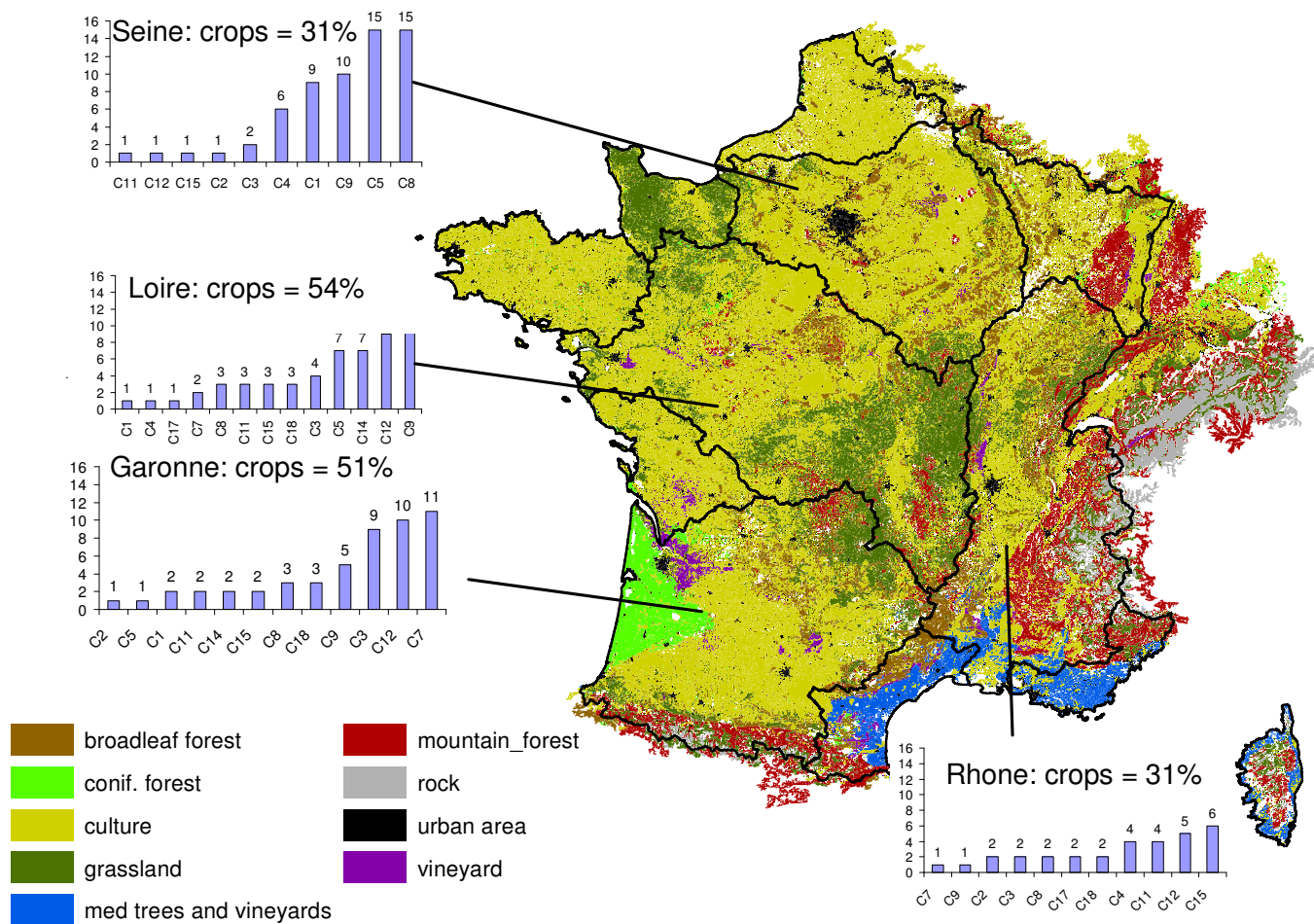


Figure 4. The main types of vegetation from the ecoclimap-france data base

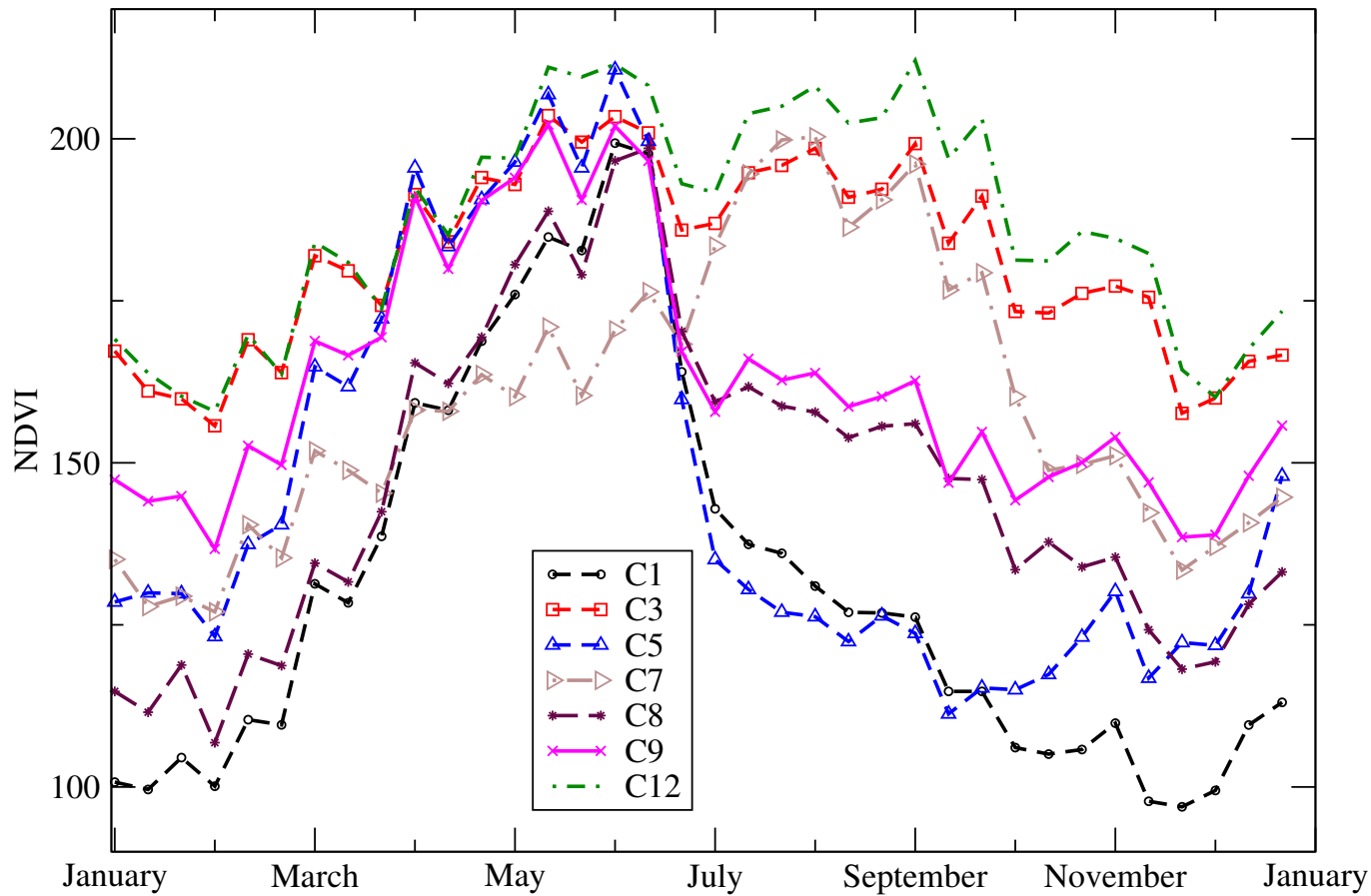


Figure 5. The 10-day evolution of the NDVI for the main crop types

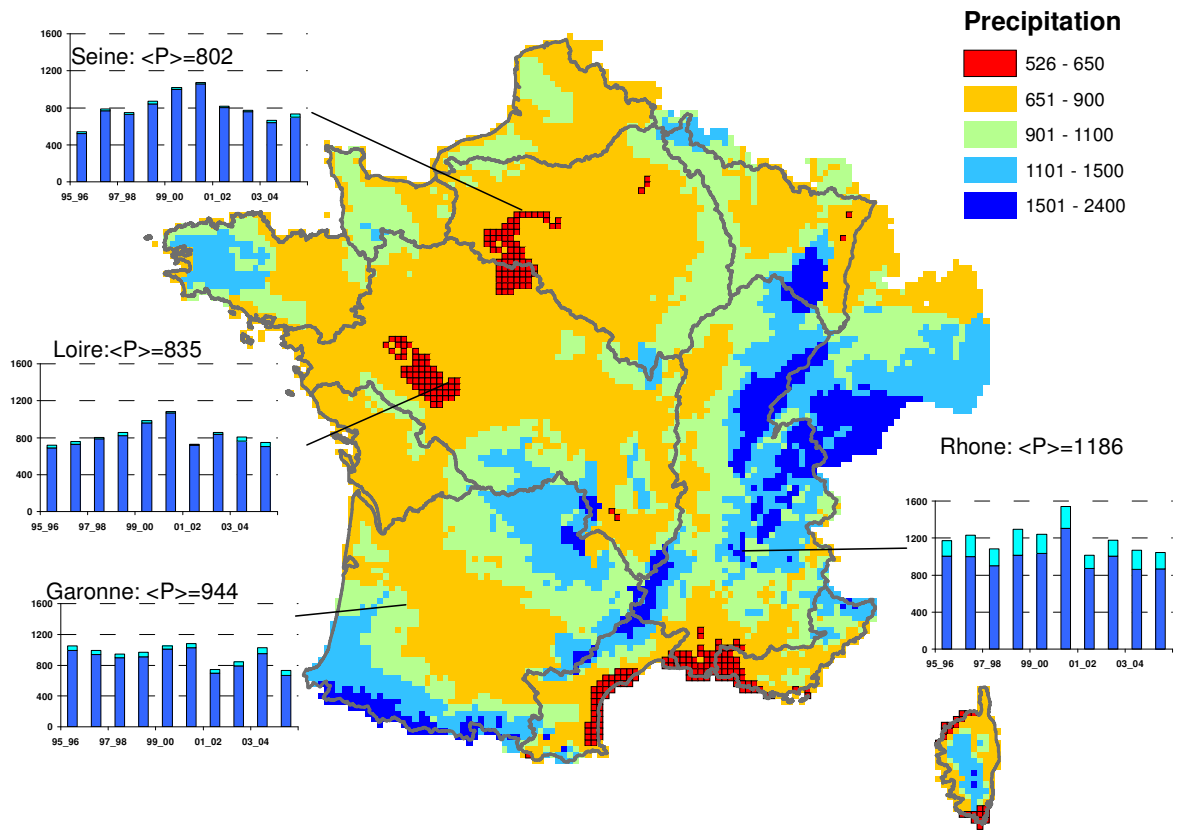


Figure 6. Mean annual precipitation in mm/year. The encapsulated graph presents the annual precipitation for each year on average over the selected basin

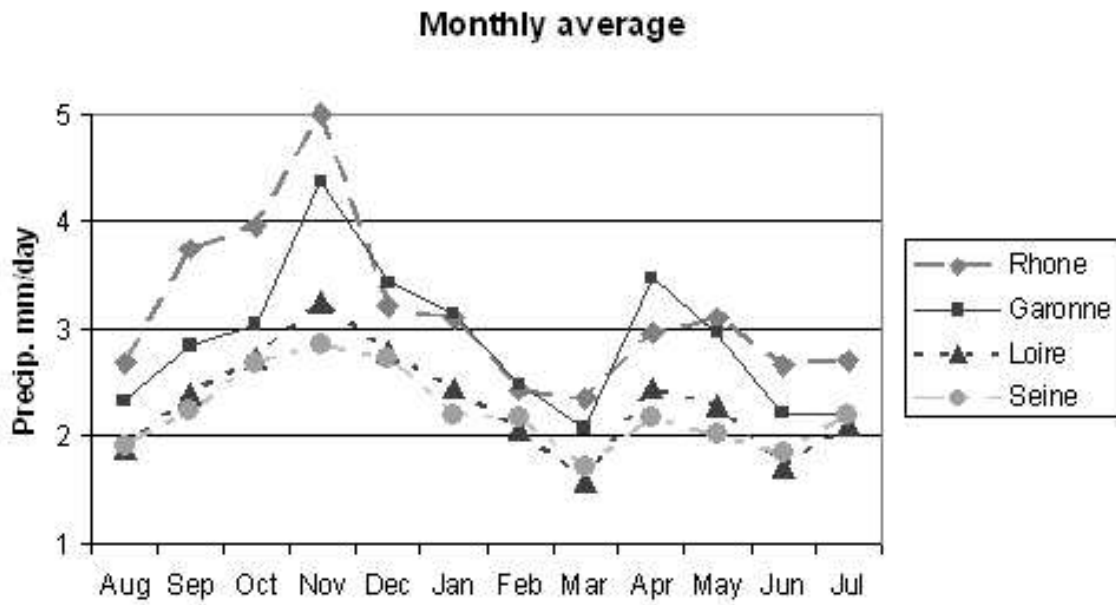


Figure 7. Mean monthly precipitation averaged on the main basin

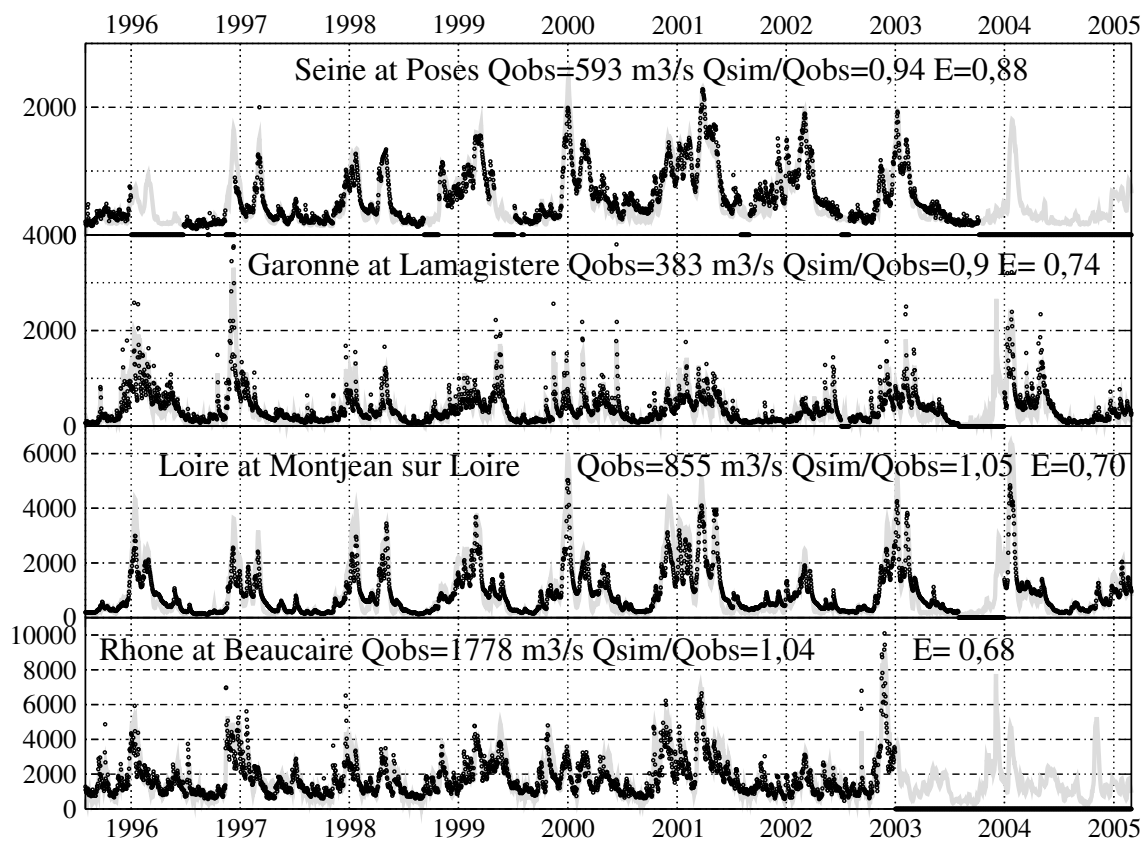


Figure 8. Daily observed (black circles) and simulated (lines) riverflows at the outlet of the four main rivers. The scale vary for each gage. The title includes the mean observed discharge on the period  $Q_{obs}$ , the discharge ratio  $Q_{sim}/Q_{obs}$  and the efficiency  $E$ .

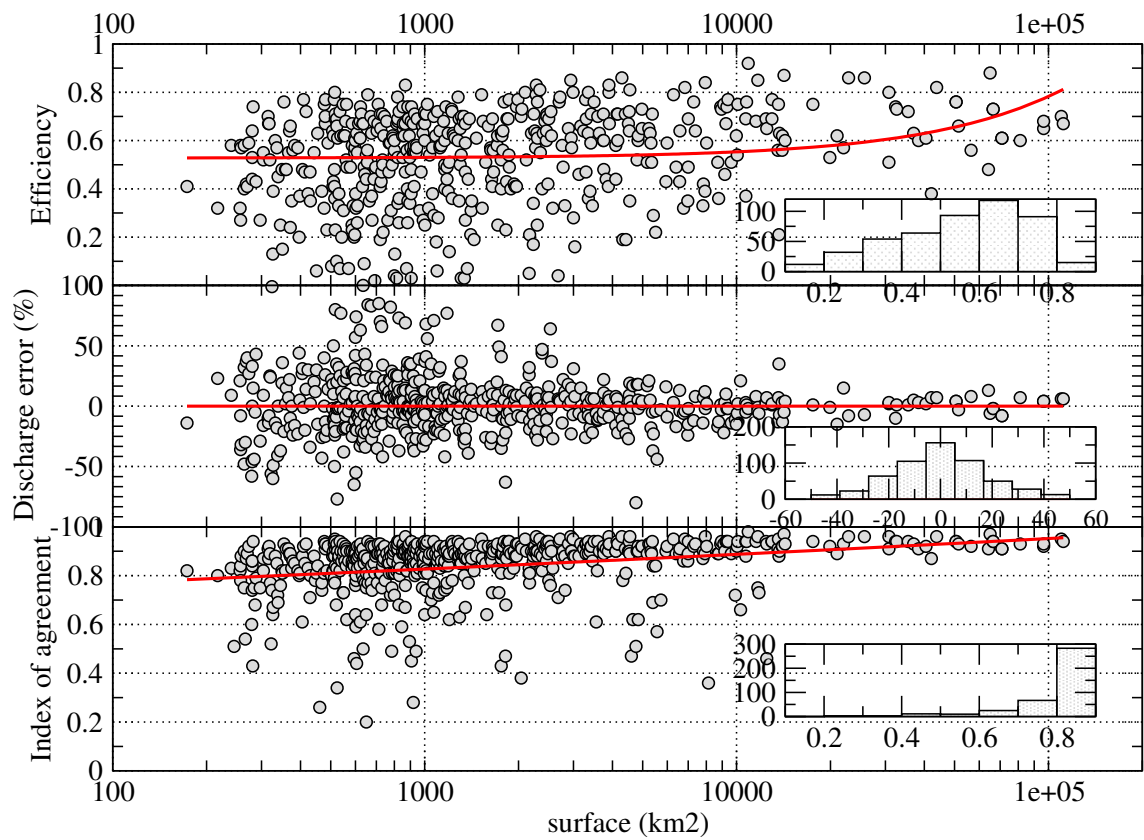


Figure 9. Efficiency (top), discharge error (middle), and index of agreement (bottom) for each simulated rivergages plotted versus the upstream area of the rivergages. The circles represent the rivergages, and the line is the linear regression (x-axis is log). The encapsulated graphs represent the histogram of the statistical results.

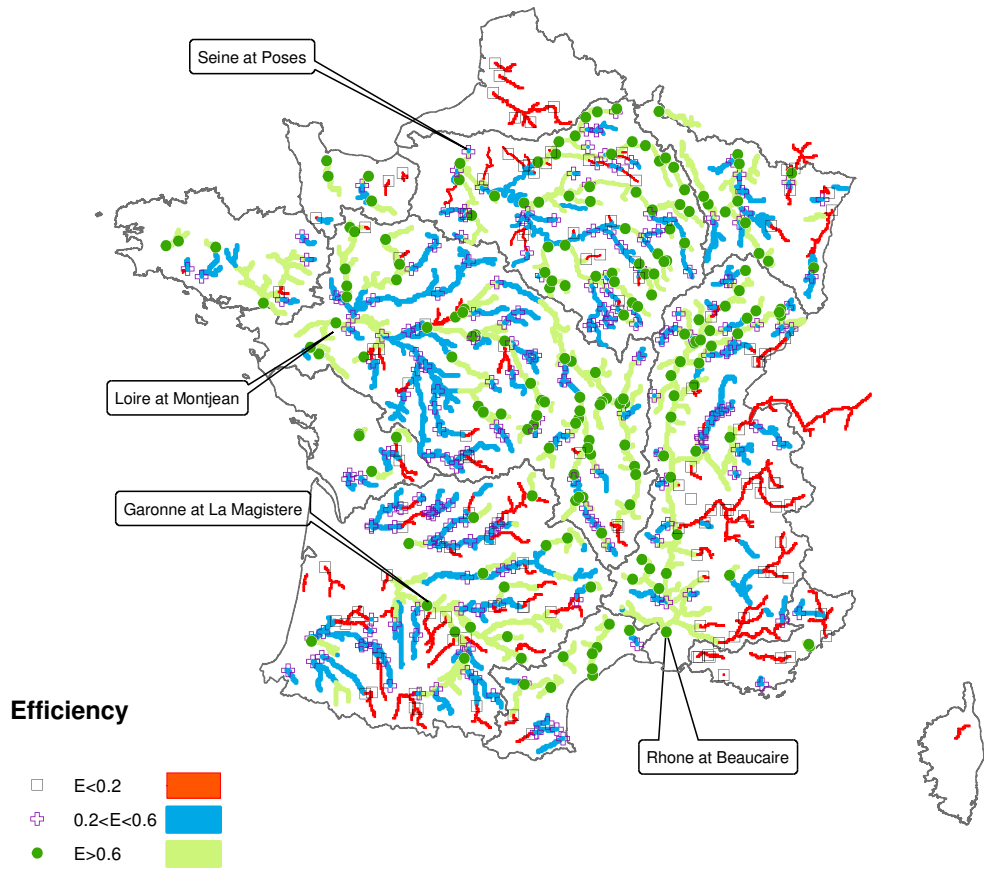


Figure 10. Spatial representation of the efficiency for each rivergage and the corresponding river network.

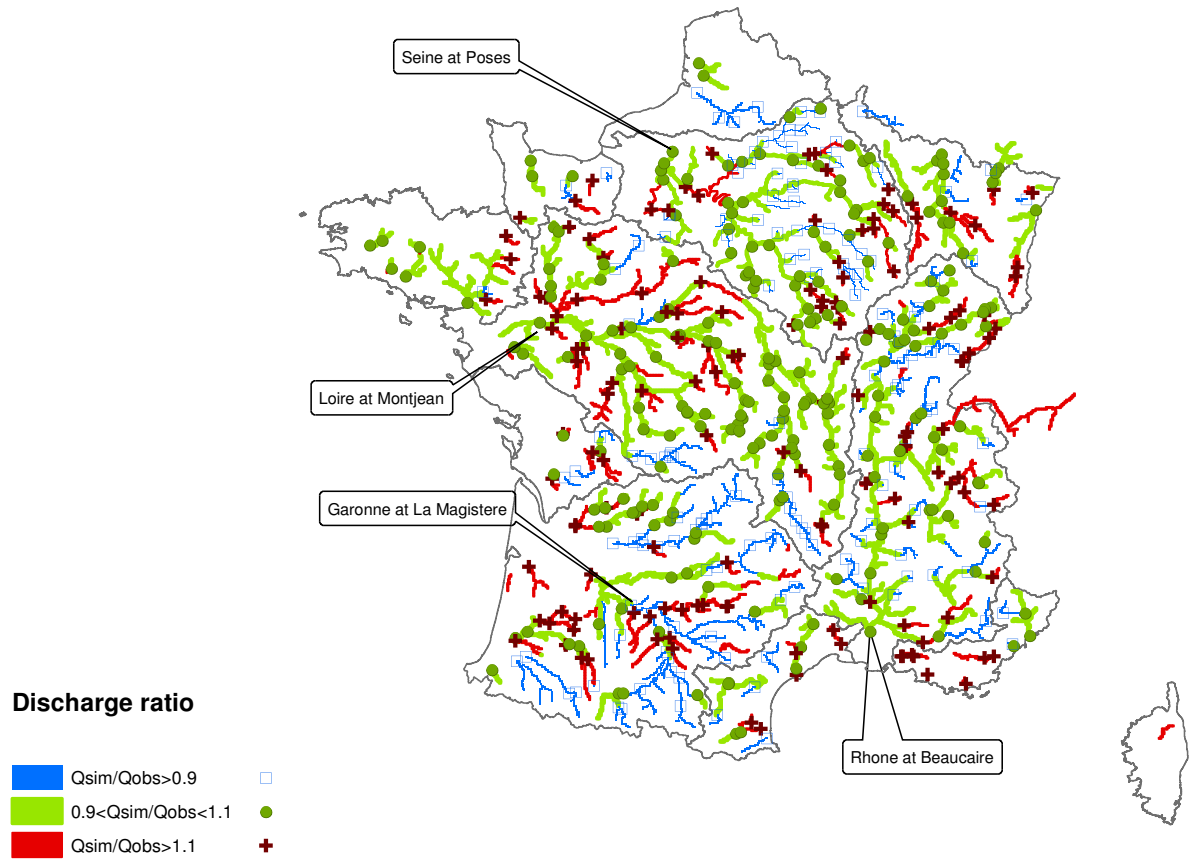


Figure 11. Spatial representation of the discharge ratio for each rivergages and the corresponding river network.



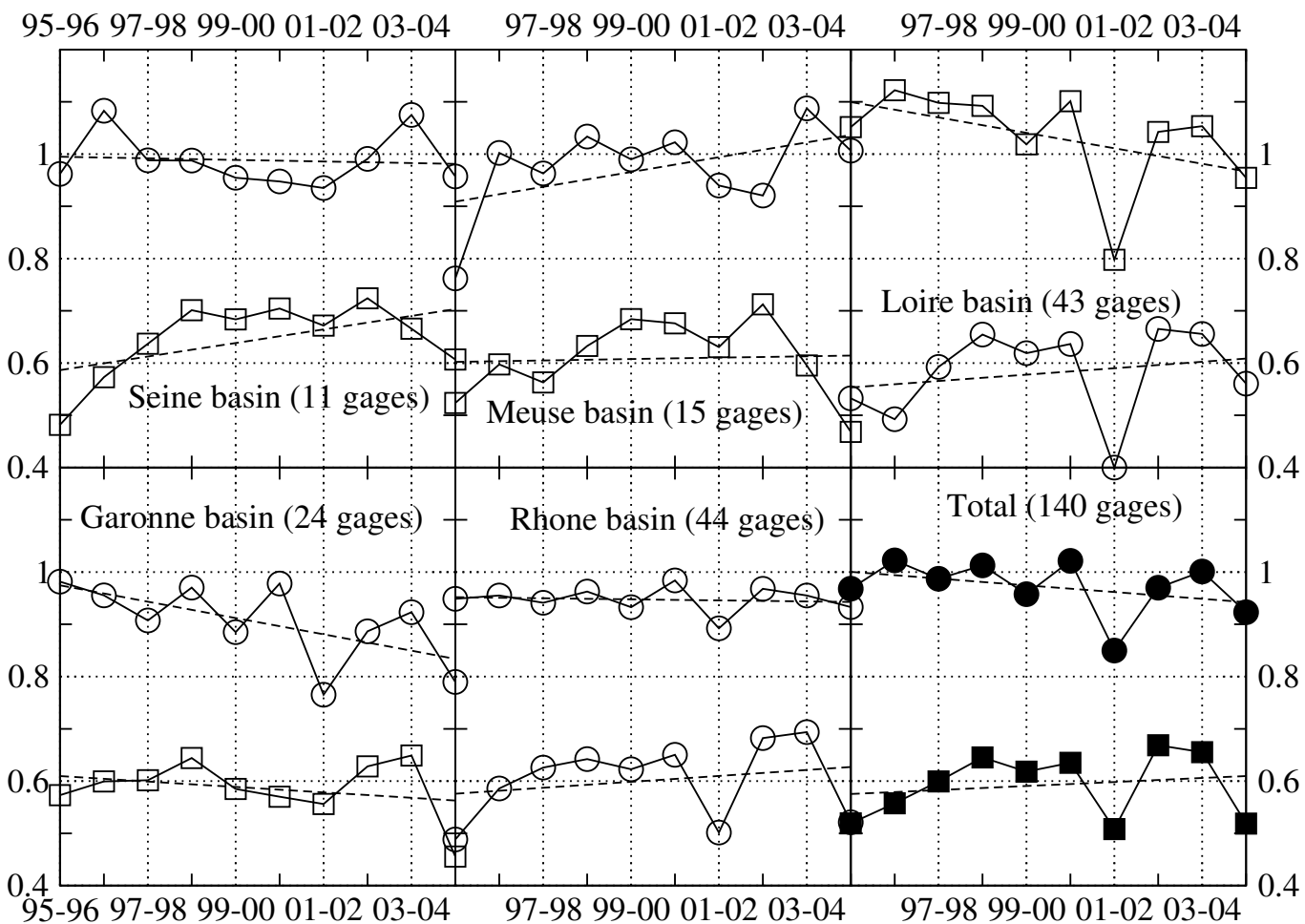


Figure 12. Evolution of the efficiency (circles) and discharge ratio (squares) on average on 5 large basins and on average for all of France. Only the rivergages with more than 200 days available each year (and with positive values of the efficiency) were taken into account. Their number is indicated on the plots

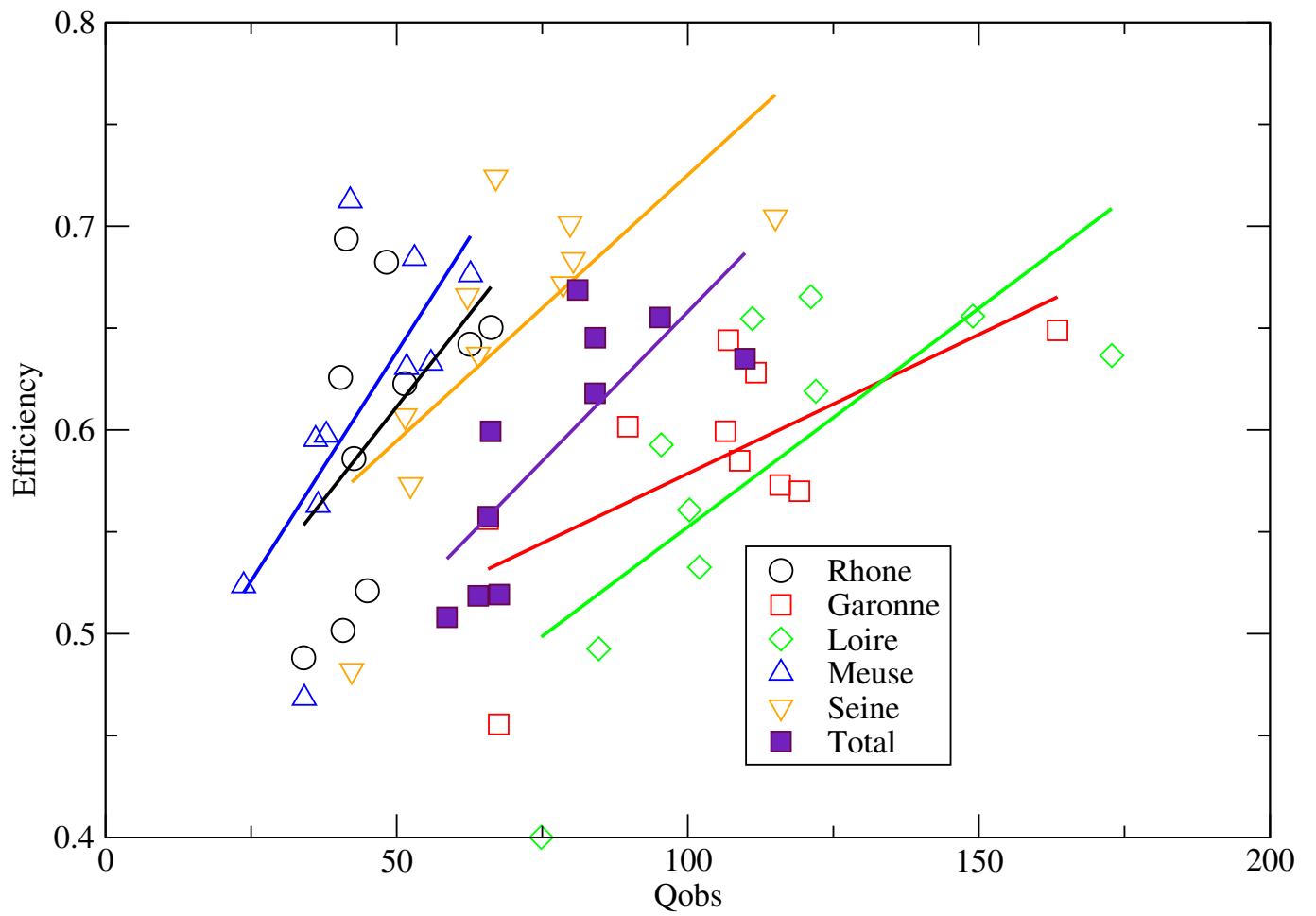


Figure 13. Relation between the efficiency and the observed discharge on average on the selected rivergages of each basin. The line correspond to the linear regression for a given basin

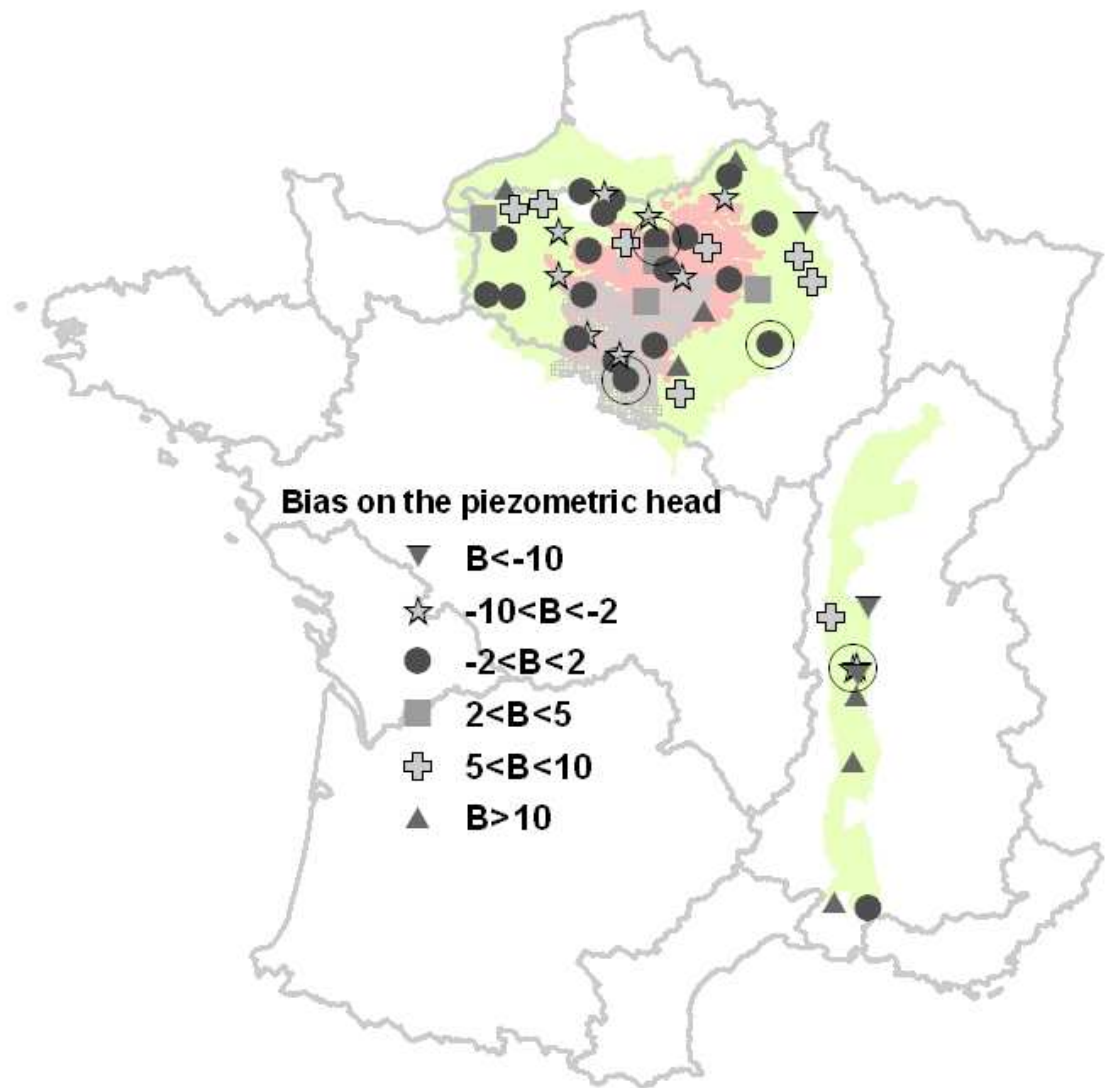


Figure 14. Spatial distribution of the bias on the 10-year simulation of the piezometric head simulated by SIM

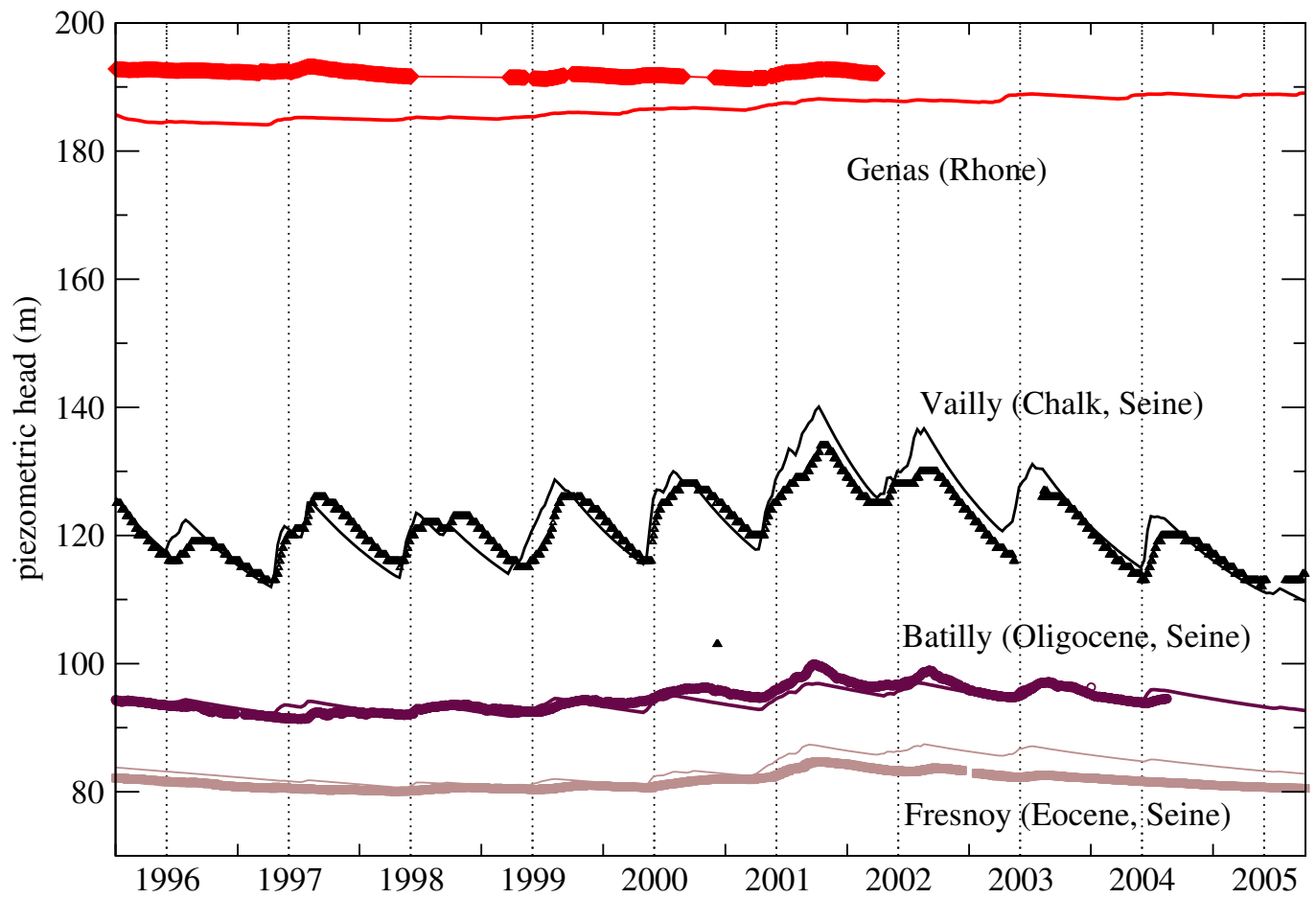


Figure 15. Evolution of the observed (symbol) and simulated (line) piezometric head for one given station over each layer of the Seine and Rhone aquifers

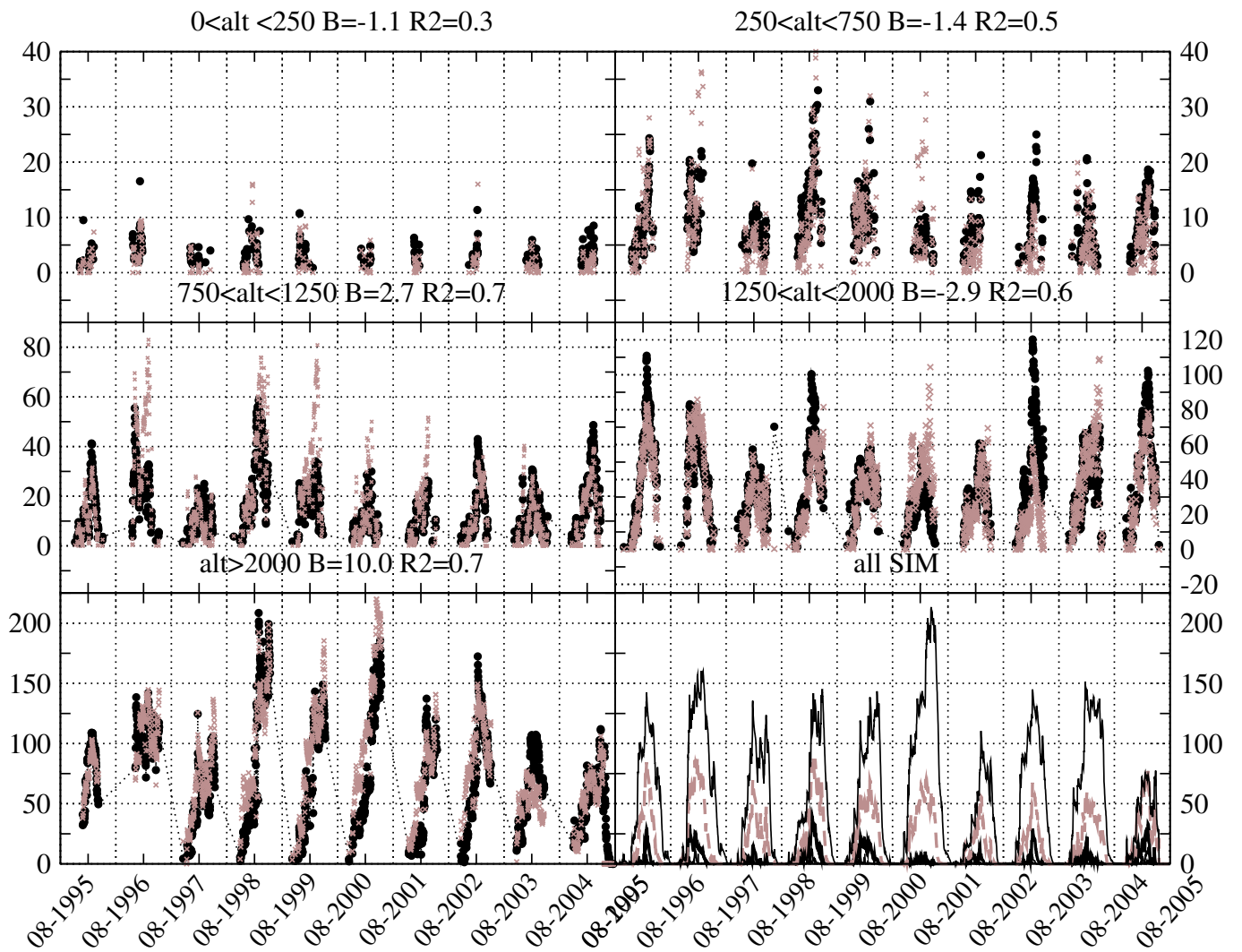


Figure 16. Snow depth observed (black dot) and simulated (cross) average on several gages according to their altitude (the average is computed each day on the stations with available data). The bottom right panel presents the evolution of the simulated snow depth on the selected stations of the 4 levels (the same number of stations is used each day to compute the average). Levels 750-1250m : black thick line; 1250-2000 gray line; over 2000m thin black line. The square correlation ( $R^2$ ) and the bias in cm ( $B$ ) are given in the subtitle



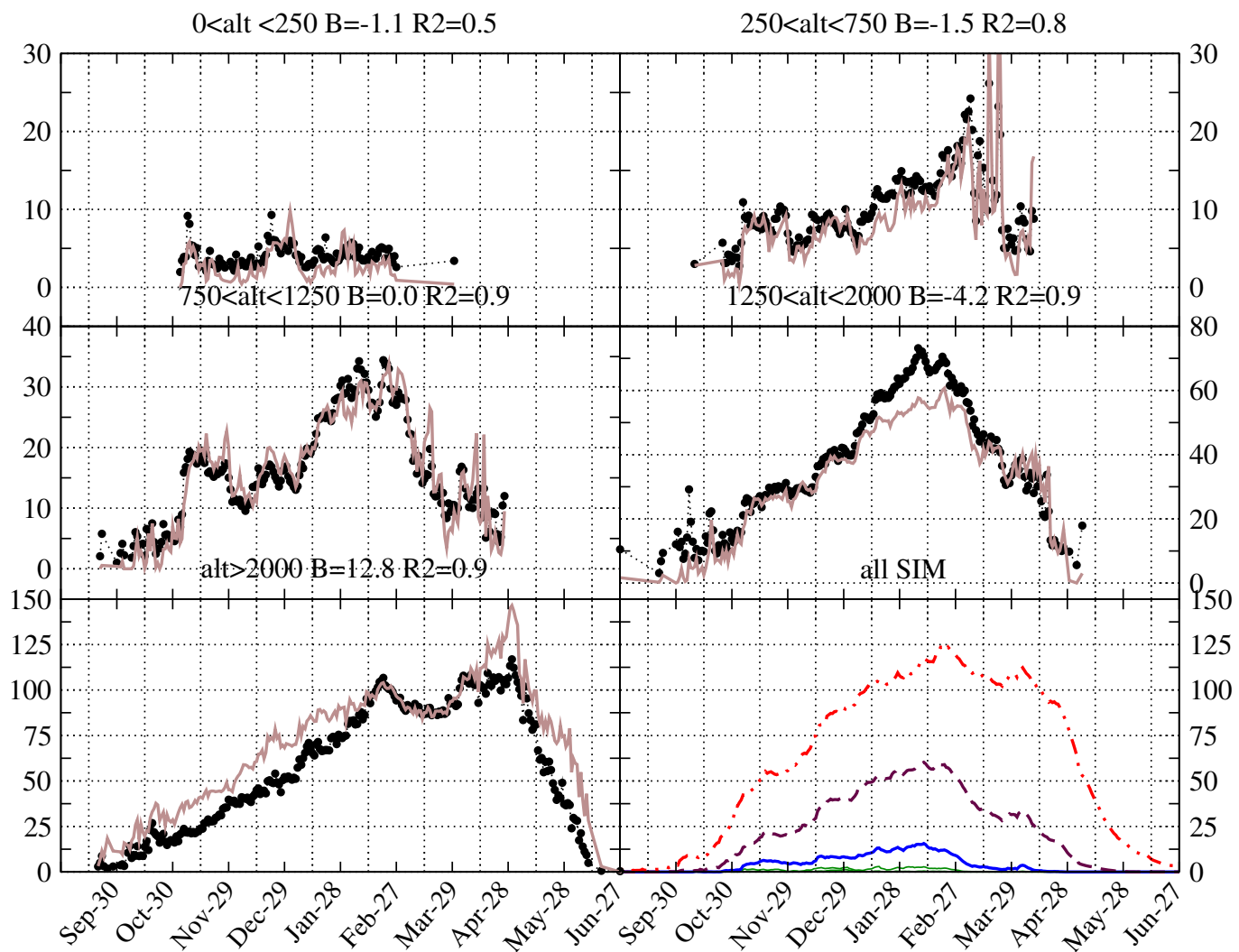


Figure 17. Same as previous figure but on average on an annual cycle

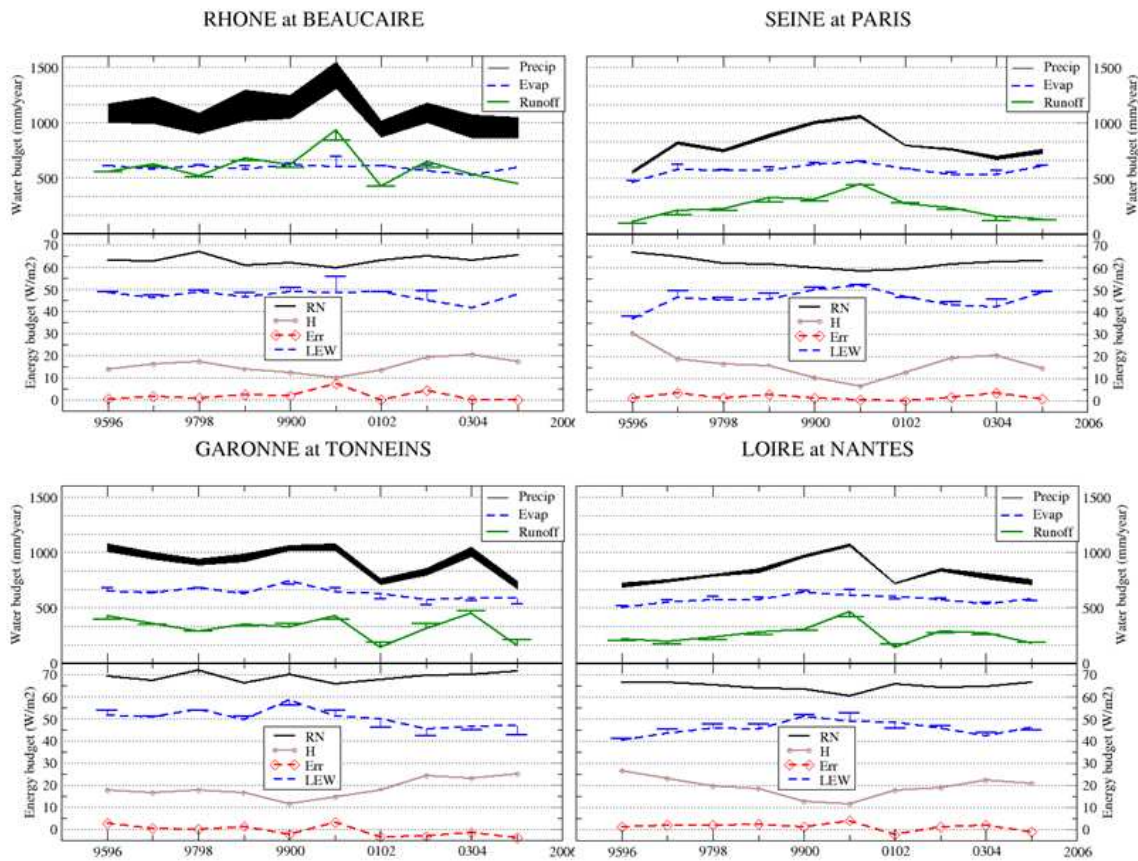


Figure 18. Water and energy budgets over the 4 main basins. The thick black lane is the total precipitation (Precip), and its thickness represents the snowfall. Evaporation (Evap), total runoff (Runoff) and latent heat flux (LEW) have an error bar that was estimated according to the error between the observed and simulated discharge. This error is shown in the energy budget panel (bottom panel) (Err) in order to compare with the net radiation (RN) and the sensible heat flux (H).



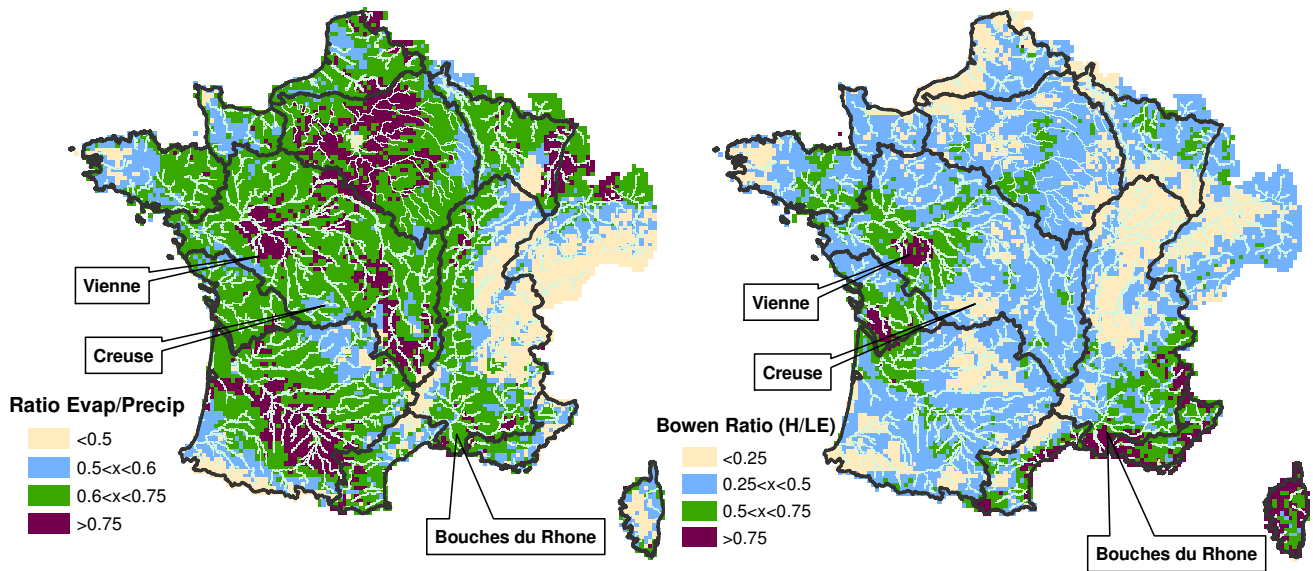


Figure 19. 10-year average bowen ratio (H/LE) (left) and 10-year average ratio of the evaporation over the precipitation (right).

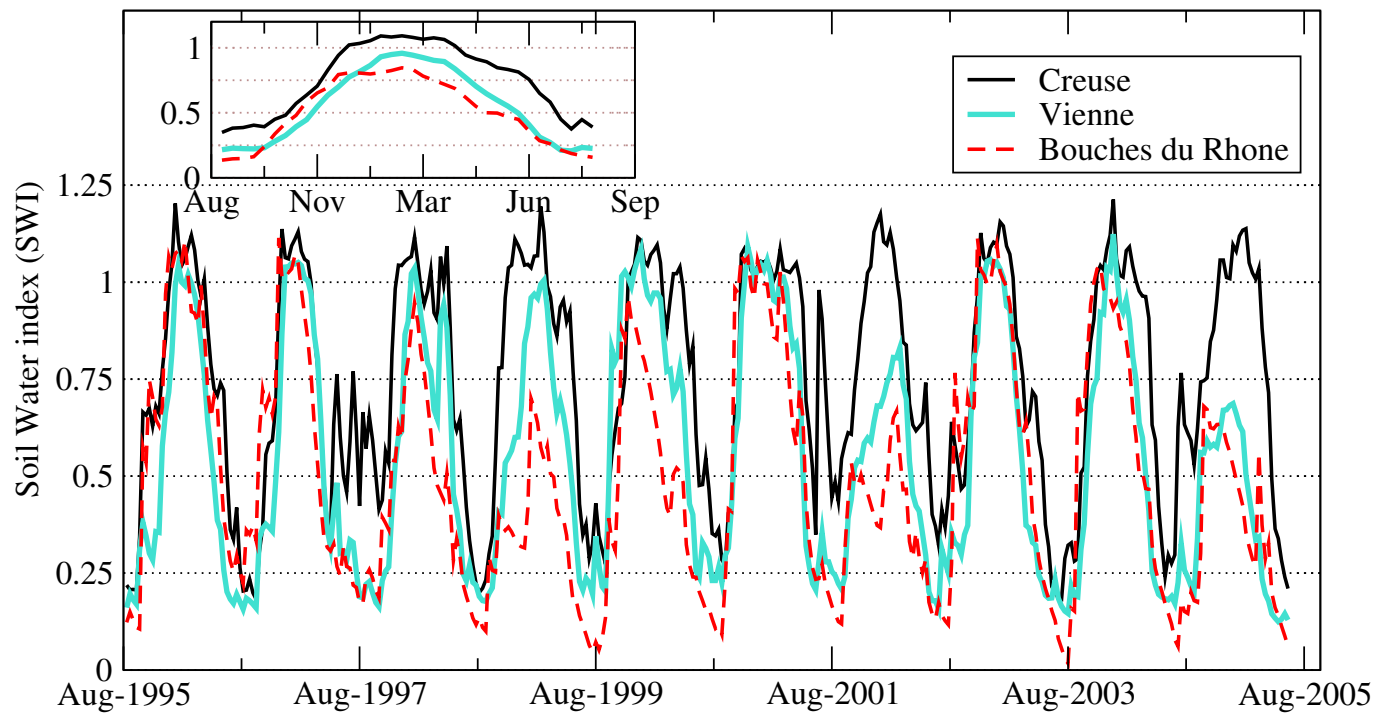


Figure 20. 10-day evolution of the soil water index (SWI) on the 3 sites plotted in figure 19. The encapsulated graph is the annual average